© 2019. Published by The Company of Biologists Ltd | Journal of Cell Science (2019) 132, jcs226514. doi:10.1242/jcs.226514

RESEARCH ARTICLE

Talin-mediated force transmission and talin rod domain unfolding independently regulate adhesion signaling

Rolle Rahikainen[1,2], Tiina Öhman[3,*], Paula Turkki[1,2,*], Markku Varjosalo[3] and Vesa P. Hytönen[1,2,‡]

ABSTRACT

Talin protein is one of the key components in integrin-mediated adhesion complexes. Talins transmit mechanical forces between β-integrin and actin, and regulate adhesion complex composition and signaling through the force-regulated unfolding of talin rod domain. Using modified talin proteins, we demonstrate that these functions contribute to different cellular processes and can be dissected. The transmission of mechanical forces regulates adhesion complex composition and phosphotyrosine signaling even in the absence of the mechanically regulated talin rod subdomains. However, the presence of the rod subdomains and their mechanical activation are required for the reinforcement of the adhesion complex, cell polarization and migration. Talin rod domain unfolding was also found to be essential for the generation of cellular signaling anisotropy, since both insufficient and excess activity of the rod domain severely inhibited cell polarization. Utilizing proteomics tools, we identified adhesome components that are recruited and activated either in a talin rod-dependent manner or independently of the rod subdomains. This study clarifies the division of roles between the force-regulated unfolding of a talin protein (talin 1) and its function as a physical linker between integrins and the cytoskeleton.

KEY WORDS: BioID, Focal adhesion, Mechanobiology, Phosphoproteomics, Protein engineering, Talin

INTRODUCTION

Focal adhesions are complex and highly dynamic structures organized around the cytosolic tails of activated β-integrin adhesion receptors (Zaidel-Bar and Geiger, 2010; Wehrle-Haller, 2012; Horton et al., 2015). Talins are focal adhesion scaffold proteins that interact with a number of adhesion proteins and regulate the nanoscale organization of the adhesion complex (Liu et al., 2015). Importantly, talins interact with both β-integrin tail domains and F-actin fibers. This mechanical linkage from the extracellular matrix (ECM) to the cell cytoskeleton is an important contributor to the integrity of the adhesion complex, and is required for persistent cell spreading and traction force generation (Zhang et al., 2008; Elosegui-Artola et al., 2016). In addition to its role as a structural scaffold, talin acts as a central adhesion complex mechanosensor. Adhesion mechanosensing by talins is known to be reflected in several essential cellular processes, such as transcription regulation through YAP/TAZ signaling, substrate sensing and cell migration (Austen et al., 2015; Elosegui-Artola et al., 2016; Rahikainen et al., 2017).

Talins contribute to adhesion mechanosignaling and to the force-regulated stabilization of adhesion complexes by at least two distinct mechanisms. First, many of the interactions of the talin rod domain are regulated by mechanical force. The transmission of sufficient mechanical force through the α-helical rod subdomains results in their unfolding (Hytönen and Vogel, 2008; del Rio et al., 2009; Margadant et al., 2011). This promotes the dissociation of some talin-bound adhesion proteins [RIAM (also known as APBB1IP), DLC1], while simultaneously revealing cryptic binding sites for other adhesion components (vinculin, actin) (del Rio et al., 2009; Goult et al., 2013; Atherton et al., 2015; Zacharchenko et al., 2016). These force-regulated interactions can directly mechanically reinforce the adhesion complex, but also mediate the recruitment of various signaling proteins, including regulators of actin and RhoGTPases (Carisey and Ballestrem, 2011). Although the reinforcement of adhesion complexes has mostly been associated with the force-regulated recruitment of vinculin, the ability of vinculin-deficient cells to polarize and migrate indicates that mechanisms independent of vinculin must contribute to adhesion reinforcement (Xu and Baribault, 1998; Thievessen et al., 2013). Second, due to the role of talins as a major structural link from β-integrin tail domains to the actin cytoskeleton, force transmission through talins regulates the dynamics of many adhesion proteins. In this way, talins also contribute to cellular mechanotransduction independently of talin rod domain unfolding (Stutchbury et al., 2017). This effect is mediated by the interactions between force-bearing adhesion and cytoskeletal proteins. For example, the catch-bond interactions between fibronectin–β1-integrin, vinculin–actin and actin–myosin are strengthened under mechanical load and thus contribute to the force-regulated stabilization of adhesion complexes (Guo and Guilford, 2006; Kong et al., 2009; Huang et al., 2017). In addition, many cellular processes are regulated by the level of mechanical tension transmitted through the actin cytoskeleton and adhesion complexes. Such processes include the assembly of fibronectin fibrils in the ECM, the severing of relaxed actin filaments by cofilins and the overall regulation of actin filament turnover (Hayakawa et al., 2011; Weinberg et al., 2017; Yamashiro et al., 2018). Through these force-dependent mechanisms, the mechanical linkage completed by a talin modulates the dynamics of adhesion proteins and regulates the stability and signaling of the adhesion complex. However, it is currently not known whether these mechanotransduction events initiated by the transmission of mechanical forces through talin can activate adhesion stabilization and downstream signaling in the absence of the talin rod subdomains. In addition, the contribution of different talin domains in the force-regulated recruitment of adhesion proteins and activation of adhesion signaling has not been thoroughly investigated.

[1]Faculty of Medicine and Health Technology and BioMediTech, Tampere University, Tampere 33014, Finland. [2]Fimlab Laboratories, Tampere 33520, Finland. [3]Institute of Biotechnology, University of Helsinki, Helsinki 00014, Finland.
*These authors contributed equally to this work

‡Author for correspondence (vesa.hytonen@tuni.fi)

V.P.H., 0000-0002-9357-1480

Received 11 October 2018; Accepted 26 February 2019

Journal of Cell Science (2019) 132, jcs226514. doi:10.1242/jcs.226514

In order to dissect the roles of talin mechanotransmission and mechanotransduction in the regulation of adhesion complex composition and signaling, we constructed modified talin proteins and analyzed their functionality in talin-null cells. We found that talin mechanotransmission contributes to adhesion stability and to the activation of adhesion phosphotyrosine signaling in the absence of talin rod domain-mediated mechanotransduction, whereas adhesion reinforcement, maturation and cell polarization are dependent on the presence of talin rod subdomains. Conversely, excess talin rod domain signaling prevents cell polarization and migration due to the loss of cellular signaling anisotropy. Strikingly, despite the observed critical importance of the talin rod subdomains in the force-regulated reinforcement of the adhesion complex, the results of this study indicate that none of the rod subdomains is indispensable for this function. This indicates that the mechanical activation of talin rod subdomains regulates adhesion reinforcement through multiple parallel mechanisms. Finally, utilizing proteomic tools, we identified novel talin-associated proteins, for which recruitment or activation is dependent either on the transmission of mechanical forces by talin or on the force-regulated unfolding of the talin rod subdomains. Overall, the results of this study open new insights into the diverse mechanisms by which talins regulate adhesion complex protein composition and signaling.

RESULTS

Talin rod domain mechanotransmission contributes to adhesion stability, but cannot mediate adhesion reinforcement and cell migration

To investigate the contribution of talin rod domain mechanotransmission and mechanotransduction in the regulation of adhesion functions, we created a series of modified talin proteins (Fig. 1A). Of these proteins, the talin head domain induces the inside-out activation of integrins, but cannot transmit mechanical forces to the actin cytoskeleton. The ΔR1-12 recombinant protein allows integrin activation and transmission of mechanical forces to the actin cytoskeleton, but does not contain any mechanoregulated rod subdomains. The ΔR1-10 and ΔR4-12 recombinant proteins transmit mechanical forces and contain two to three rod subdomains with different mechanical properties and mechanically regulated interaction sites (Haining et al., 2016). All recombinant talin forms were C-terminally tagged with mCherry fluorescent protein and expressed in *Tln1*$^{-/-}$*Tln2*$^{-/-}$ cells deficient of both endogenous talin-1 and talin-2 (Theodosiou et al., 2016). The correct expression of all talin forms was confirmed by western blotting (Fig. S1A).

As expected, the expression of the talin head domain in talin-deficient cells promoted cell attachment to ECM proteins and isotropic cell spreading (Fig. 1B), but did not allow cell polarization (Fig. 1D) or migration (Fig. 1E) (Zhang et al., 2008). Although the ΔR1-12 protein significantly increased cell-spreading area compared to talin head domain, it too failed to support cell migration. In contrast, all three talin forms containing rod subdomains facilitated cell spreading, polarization and migration (Fig. 1C–E; Movie 1). This indicates that, in *in vitro* conditions, either the R1-3 or the R10-12 subdomains are sufficient to reinforce adhesion complexes and facilitate cell polarization and migration. Analyses of lamellipodium actin retrograde flow rate (Fig. 1F) and macroscopic collagen gel contraction (Fig. 1G) revealed that, while the actin-binding site (ABS3) present in the ΔR1-12 protein was able to slow down actin retrograde flow, the ΔR1-12 protein was unable to support adhesion reinforcement and traction force generation. However, cells expressing this talin protein readily relocated fluorescent fibronectin molecules coated on glass coverslips (Fig. S1G), indicating that the ECM–integrin–talin–actin clutch is indeed engaged in these cells.

As expected, fluorescence recovery after photobleaching (FRAP) experiments for adhesion-localized talin revealed increased adhesion turnover for talin head and the ΔR1-12 protein compared to wild-type talin (Fig. 1H). Strikingly, in fluorescence live-cell imaging, the adhesions formed around either the talin head domain or the ΔR1-12 protein remained in their original positions over the 120-min time-lapse series (Fig. 1I; Fig. S1H). This was in marked contrast to the sliding and highly dynamic adhesions present in cells expressing wild-type talin and suggests that talin rod domain unfolding is not only required for adhesion stabilization, but also for their controlled disassembly. Overall, these results demonstrate that, even in the absence of talin rod domain mechanotransduction, the transmission of mechanical force through the talin protein contributes to adhesion stabilization, presumably through the stabilization of catch-bond interactions between force-bearing adhesion proteins (Kong et al., 2009). However, the lack of cell migration or macroscopic collagen contraction by the ΔR1-12 protein suggests that, in the absence of talin rod domain-mediated adhesion reinforcement, the adhesion complex repeatedly fails under mechanical tension.

Vinculin is one of the best-characterized talin-binding proteins and its interaction with talin protein is known to require the mechanical activation of the talin rod subdomains (Hytönen and Vogel, 2008; del Rio et al., 2009). As expected, cells expressing the talin head domain or the ΔR1-12 protein were unable to recruit vinculin into adhesion sites (Fig. 1J,L; Fig. S1I), while the ΔR1-10 [two vinculin-binding sites (VBSs)] and ΔR4-12 (six VBSs) proteins and wild-type talin (11 VBSs) each recruited vinculin to levels roughly reflecting the number of mechanically regulated VBSs in these talin forms (Fig. 1L). Similar differences in vinculin recruitment were also seen after normalizing the results to the level of talin protein in each adhesion (Fig. 1K,M), indicating that the composition of the talin rod domain determines the level of vinculin recruitment into the adhesion complex.

Mechanical activation of talin rod subdomains is required for their function in adhesion stabilization

Because adhesion reinforcement and cell polarization were found to depend on the presence of talin rod subdomains, we were curious to see whether the mere presence of the R1-3 subdomains is sufficient for cell polarization, or if the mechanical activation of these subdomains is necessary for their functions. To study this, we designed an expression construct composed of the talin ΔR1-12 protein C-terminally fused with the R1-3 subdomains (R1-12+C-terminal R1-3) (Fig. 2A; Fig. S1B). When expressed in *Tln1*$^{-/-}$*Tln2*$^{-/-}$ cells, this reorganized talin induced isotropic cell spreading identical to the phenotype induced by the ΔR1-12 protein lacking most of the rod domain (Fig. 2A,B; Movie 2). Moreover, the cells expressing the permuted ΔR1-12+C-terminal R1-3 protein were unable to migrate on fibronectin-coated glass coverslips (Fig. 2D; Movie 2), indicating that the mechanical activation of the rod subdomains is indispensable for their function in the reinforcement of the adhesion complex.

As expected, the ΔR1-12+C-terminal R1-3 talin could not recruit endogenous vinculin into adhesion sites (Fig. 2A). However, co-expressed full-length vinculin or its autoinhibition-deficient T12 mutant (Cohen et al., 2005) readily localized into adhesion sites in these cells and promoted their polarization (Fig. S2A). Although the activity of talin VBSs is essentially regulated by mechanical force, these results indicate that, even in the absence of mechanical tension, an excess of cytosolic vinculin can shift the equilibrium of

Journal of Cell Science (2019) 132, jcs226514. doi:10.1242/jcs.226514

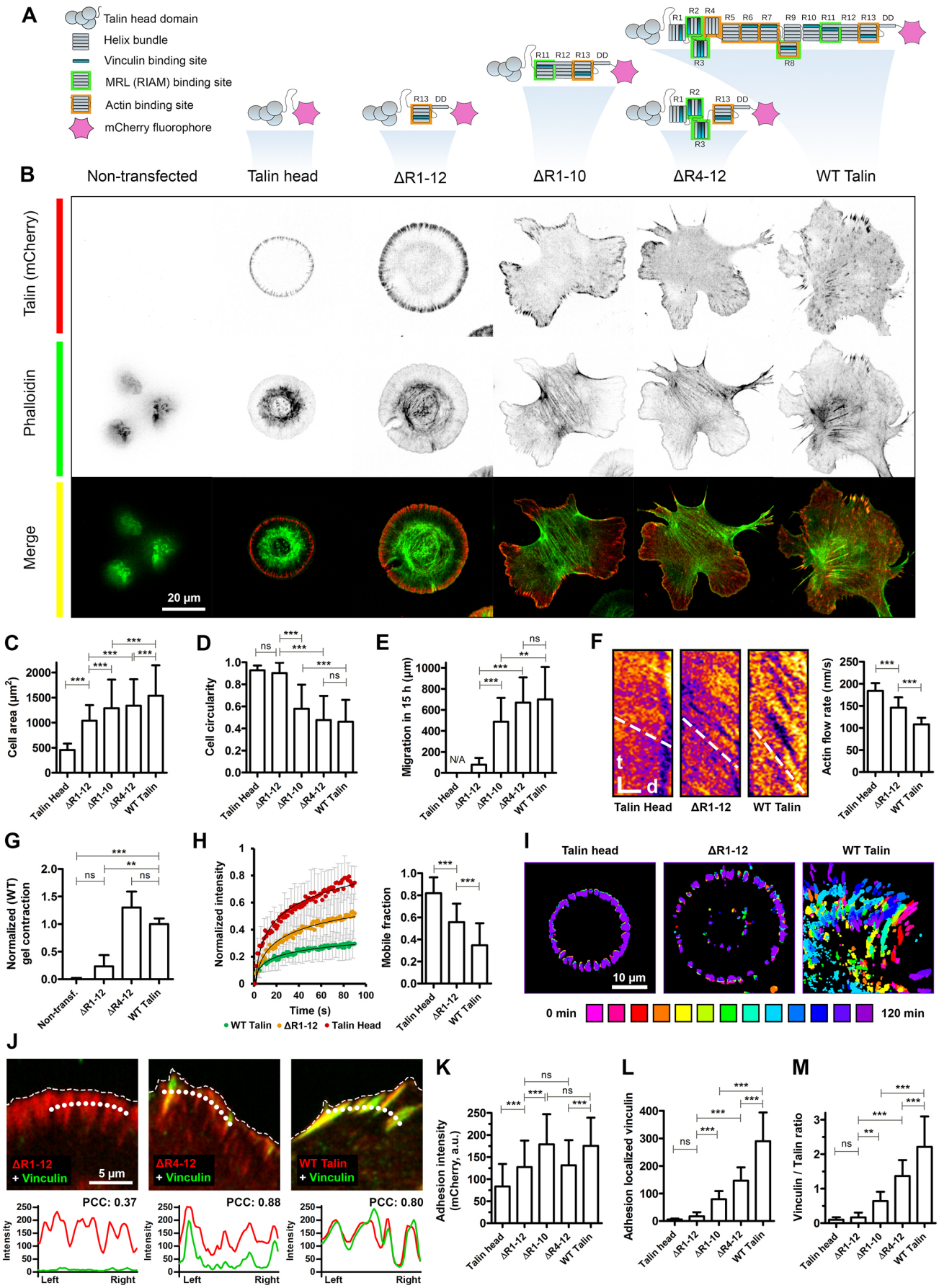

Fig. 1. See next page for legend.

Journal of Cell Science (2019) 132, jcs226514. doi:10.1242/jcs.226514

Fig. 1. Talin rod domain mechanotransmission contributes to adhesion stability but cannot mediate adhesion reinforcement and cell migration. (A) Schematic illustration of the truncated talin proteins expressed in *Tln1*$^{-/-}$*Tln2*$^{-/-}$ cells. The binding sites for selected talin ligands identified in previous studies are shown for talin rod. (B) Representative images of cells expressing truncated talin proteins. Phalloidin staining was used to visualize actin cytoskeleton. (C,D) Cell area and circularity analysis for *Tln1*$^{-/-}$*Tln2*$^{-/-}$ cells expressing truncated talin proteins. *n*=288–436 cells pooled from two independent experiments. (E) Cell migration analysis for random migration. *n*=10–87 cells for each talin protein pooled from three independent experiments. Also see Movie 1. (F) The rate of actin retrograde flow in lamellipodia. Vertical scale bar: 10 s; horizontal scale bar: 2 µm. *n*=63 kymographs from 21 cells for each talin protein. The dashed lines indicate actin flow rate in representative kymograms. (G) Contraction of collagen-I matrix in 72 h. Results normalized to wild-type (WT) talin. *n*=12–20 collagen-I matrices from three to five independent experiments. (H) FRAP recovery curves and mobile fractions. *n*=20–27 cells from two independent experiments. (I) Overlaid images at 10-min intervals from 120 min fluorescent live-cell imaging. Thresholded images at each time point are presented with different colors. See Fig. S1H for individual frames. (J) Vinculin colocalization with talin. See Fig. S2I for representative images. Intensities of talin and vinculin were measured along 10-µm selections (dotted lines) and plotted as line graphs (below). PCC, Pearson correlation coefficient. The dashed white lines indicate the cell edge. (K) Analysis of the relative intensities of adhesion-localized talin proteins. Intensity values were normalized to the cytosolic background fluorescence in each cell and presented relative to the WT talin intensity. *n*=53–61 cells pooled from four independent experiments. (L) Fluorescence intensity analysis for adhesion-localized vinculin. *n*=23–34 cells pooled from two independent experiments. (M) Vinculin/talin intensity ratio for the graphs in K and L. *n*=23–34 cells pooled from two independent experiments. Data are mean±s.d. The statistical significance of all results was analyzed by one-way ANOVA and Bonferroni test. ns, not significant; ***P*<0.01, ****P*<0.001.

folded and unfolded talin conformations towards the unfolded form. Once bound to a talin, vinculin can function as a linkage between the talin and actin, thus mediating the force-regulated activation of the other VBSs in the talin rod domain and allowing cell polarization. These results indicate the dynamic equilibrium between active and inactive conformations of talin rod subdomains to be regulated by both mechanical forces and the cytosolic concentration of talin-binding proteins.

To confirm the role of the C-terminal actin-binding site (ABS3) in talin R13 in the initial mechanical activation of the talin rod, we created talin ΔR13-DD mutant lacking the R13 subdomain (Fig. 2E; Fig. S1C). *Tln1*$^{-/-}$*Tln2*$^{-/-}$ cells expressing this mutant were unable to spread, polarize or migrate, and exhibited an overall phenotype similar to that of cells expressing the talin head domain (Fig. 2F–H). Surprisingly, in contrast to the ΔR1-12+C-terminal R1-3 protein, co-expression of vinculin did not rescue the polarization of the cells expressing the ΔR13-DD protein (Fig. S2B). This may be explained by the autoinhibition between the talin head domain and R9 subdomain in the ΔR13-DD protein, or by decreased stability of the R3 subdomain in the ΔR1-12+C-terminal R1-3 protein in the absence of the flanking R4 subdomain. Overall, these results indicate that, while the ABS2 in the subdomains R4-R8 is known to be required for the generation of high traction forces (Atherton et al., 2015), ABS3 in the R13 subdomain is indispensable for the initial talin activation, adhesion stabilization and cell spreading.

The force-regulated unfolding of talin rod subdomains generates the signaling anisotropy required for cell polarization and migration

Although the mechanical loading of integrins by ECM ligands is known to regulate cell polarity, the contribution of talin rod mechanosensing in this process has not been elucidated (Prager-Khoutorsky et al., 2011; Bun et al., 2014). To investigate the possible role of force-regulated unfolding of talin rod subdomains in the regulation of cell polarity, we utilized the destabilized ΔR1-12 (4S) protein developed in a previous study (Rahikainen et al., 2017). The facilitated unfolding of this destabilized protein was found to severely impair cell polarity and the rate of cell migration (Fig. 2K,L). To study whether the loss of cell polarity was caused by insufficient adhesion stability or by the lack of cellular signaling anisotropy, we created tandem constructs composed of the destabilized ΔR4-12 (4S) protein supplemented by either one [ΔR4-12 (4S)+R1-3] or two [ΔR4-12 (4S)+2xR1-3] additional R1-3 fragments (Fig. 2I). Altogether, the addition of one R1-3 fragment significantly facilitated cell polarization and migration, but was not sufficient to completely rescue the effects of talin destabilization. However, the addition of two R1-3 fragments fully rescued cell spreading, polarization and migration (Fig. 2J–L). As each of these talin forms contains the same destabilized R3 subdomain, these results indicate that the facilitated unfolding of the R3 subdomain does not prevent cell polarization and migration in the presence of intact R3 subdomains with sufficient mechanical stability. Instead, the excess activity of the ΔR4-12 (4S) form seems to disturb cell polarization by preventing the correct spatial regulation of adhesion reinforcement and signaling. Although the talin tandem proteins themselves were recruited to adhesions roughly to the same extent as the destabilized ΔR4-12 (4S) form, they caused a further increase in the level of adhesion-recruited vinculin and increased vinculin/talin ratio in the adhesion sites (Fig. 2M–O; Fig. S2C). This indicates that the additional VBSs in the tandem proteins are activated by mechanical tension, which restores the cellular anisotropy of vinculin recruitment and adhesion signaling. Thus, while the establishment of cell polarity does not seem to be dependent on the absolute level of talin in the adhesion complex, the correct force-regulated control of its unfolding is indispensable for cell polarity. Taken together, these results reveal that the spatially restricted unfolding of the talin rod domain is required for the generation of cellular signaling anisotropy. This anisotropy is critical for the establishment of cell front-back polarity, as well as for cell migration.

Talin force transmission regulates adhesion complex composition and signaling independently of talin rod subdomains

Talin is known to mediate the recruitment and release of adhesion proteins in a force-dependent manner (Gough and Goult, 2018); however, the contribution of talin mechanotransmission in the regulation of adhesion complex protein composition and signaling has remained unknown. To investigate how the adhesion complex protein composition is regulated by talin force transmission and the unfolding of rod subdomains, we used a proximity biotinylation approach, called BioID (Roux et al., 2018), together with affinity purification and mass spectrometry (MS) (Table S1). This analysis revealed a group of proteins recruited to the adhesion complex only in cells expressing wild-type talin (Fig. S3A). These include several expected hits, such as members of the cortical microtubule stabilization complexes (CMSCs), including the Kank2 protein known to mediate the interaction between CMSCs and the talin R7 subdomain (Sun et al., 2016). Interestingly, the tumor suppressor protein testin was also among the proteins recruited by wild-type talin. Immunofluorescence was used to confirm that its previously proposed (Coutts et al., 2003; Sala et al., 2017), but poorly understood, interaction with talin is indeed mediated by the talin rod domain (Fig. S3D).

Several of the detected proteins had increased biotin labeling in cells expressing the ΔR1-12 protein (Fig. S3B). This indicates that

Journal of Cell Science (2019) 132, jcs226514. doi:10.1242/jcs.226514

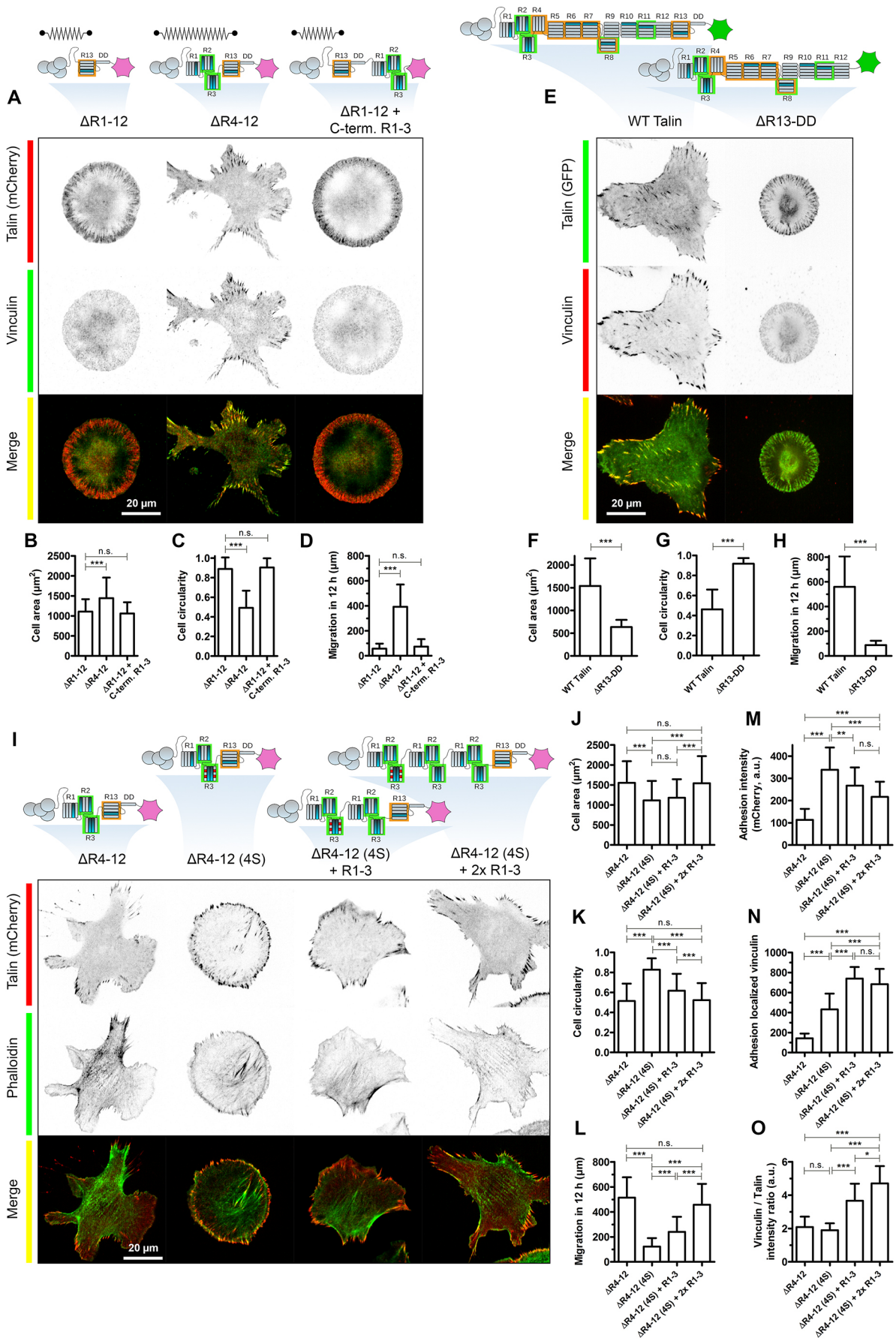

Fig. 2. See next page for legend.

Journal of Cell Science (2019) 132, jcs226514. doi:10.1242/jcs.226514

Fig. 2. The force-regulated unfolding of the talin rod domain generates the signaling anisotropy required for cell polarization and migration. (A) Representative images of cells expressing reorganized talin proteins. The spring symbols indicate the path of force transmission in each protein. Note how the two latter proteins contain the same talin R1-3 rod domain fragment but in stretchable (ΔR4-12) or in non-stretchable (ΔR1-12+C-terminal R1-3) organization. (B,C) Cell circularity and cell surface area analysis for cells expressing reorganized talin proteins. *n*=221–231 cells for each protein. (D) Cell migration analysis. *n*=64–91 cells for each talin protein. Also see Movie 2. (E) Representative images of cells expressing WT talin-GFP or the ΔR13-DD protein. (F,G) Cell circularity and cell surface area analysis for cells expressing the ΔR13-DD protein. *n*=283 and 152 cells for WT and ΔR13-DD, respectively. (H) Migration analysis for ΔR13-DD. *n*=30 and 36 cells for WT and ΔR13-DD, respectively. (I) Representative images of cells expressing destabilized and tandem talin proteins. (J,K) Cell circularity and cell surface area analysis for the modified talin proteins presented in I. *n*=201–232 cells for each talin protein pooled from two independent experiments. (L) Cell migration analysis. *n*=33–98 cells for each talin protein pooled from two independent experiments. Also see Movie 3. (M) Fluorescence intensity analysis for adhesion localized talin proteins. *n*=24–44 cells for each talin protein pooled from three independent experiments. (N) Fluorescence intensity analysis for adhesion localized endogenous vinculin. *n*=11–29 cells for each talin protein pooled from two independent experiments. (O) Vinculin/talin intensity ratio for the graphs in M and N. *n*=11–29 cells for each talin protein. Data are mean±s.d. The statistical significance of all results was analyzed by one-way ANOVA and Bonferroni test. n.s., not significant; **P*<0.05, ***P*<0.01, ****P*<0.001.

the recruitment of these proteins into the proximity of adhesion complex is dependent on the transmission of mechanical forces, but independent of the presence of rod subdomains. Many of the proteins identified in the BioID analysis, including focal adhesion kinase (FAK; also known as PTK2), p130Cas (also known as BCAR1), p120Ctn (also known as CTNND1) and paxillin, are involved in adhesion phosphotyrosine signaling. This suggests that the transmission of mechanical forces through the ΔR1-12 protein regulates adhesion phosphotyrosine signaling independently of talin rod domain unfolding. However, because of the continuous biotin labeling of adjacent proteins over time, BioID is inherently sensitive to any differences in the turnover rates of the studied proteins. Therefore, it seems possible that the observed differences are caused, in part, by differences in adhesion turnover. Furthermore, some canonical focal adhesion proteins including vinculin, VASP and Enah were detected similarly in the proximity of different talin forms and the negative control (Fig. S3C), suggesting that high cytosolic concentrations of specific adhesion proteins may cause a high background signal in BioID analysis. Finally, due to the elongated conformation of activated talin, differences in the length of the studied talin forms may be reflected in the labeling efficiencies of adhesion proteins interacting with different talin domains.

To investigate the talin-dependent regulation of adhesion signaling events in more detail, we performed phosphopeptide enrichment, followed by high-resolution MS-based quantitative phosphoproteome analysis for whole-cell lysates of *Tln1*$^{-/-}$*Tln2*$^{-/-}$ cells expressing either talin head domain, ΔR1-12 or wild-type talin-1 (Table S2). Over 359 sites in 264 proteins were common for all expressed talin constructs, but not detected in control samples, indicating dependence on the talin head domain, but independence of both talin mechanotransmission or rod mechanotransduction (Fig. 3A; Table S3). The most enriched gene ontology (GO) term for this group was 'cell–cell adhesion' and included many cell adhesion and cytoskeletal proteins, such as PAK4 (pS181), plectin (pS4627/pS4629), Mark2 (pS483) and talin-1 (pS425) itself. Nearly 141 sites in 110 proteins were detected in cells expressing ΔR1-12 or wild-type talin, but not in cells transfected with the talin head domain or empty vector, indicating that their phosphorylation is dependent on the transmission of mechanical forces, but not on talin rod mechanotransduction. These hits included proteins involved in the regulation of Rho-family GTPases, such as

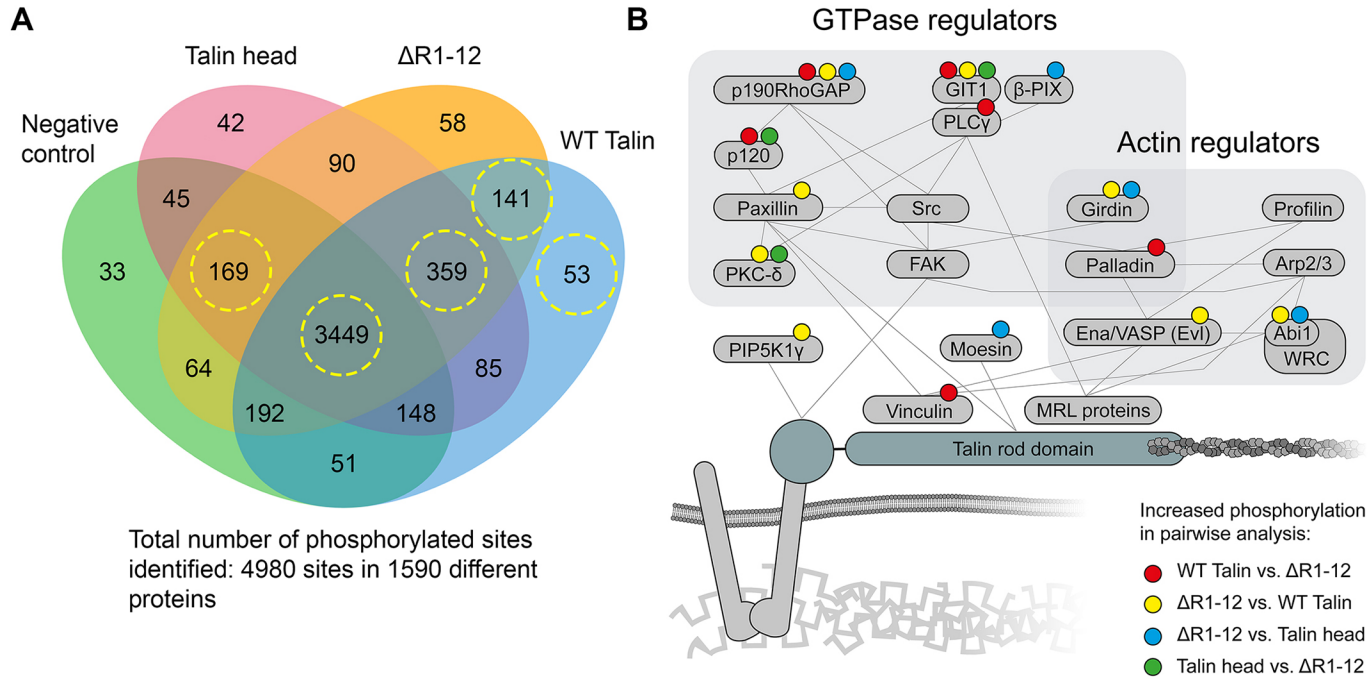

Fig. 3. Phosphoproteome analysis for cells expressing modified talin proteins. (A) Venn diagram illustrating the overlap of phosphorylated sites detected in whole-cell lysates using MS/MS. Yellow dashed circles indicate the groups analyzed by functional annotation enrichment analysis (Table S4). (B) Pairwise analysis of the immediate downstream signaling pathways for the talin protein. Significant enrichment (5-fold cutoff) of one or more phosphorylation sites in each protein is indicated by colored dots. The specific sites phosphorylated in each protein are presented in Table S7.

Journal of Cell Science (2019) 132, jcs226514. doi:10.1242/jcs.226514

p190RhoGAP (pY1105), Syde1 (pS231/pS244), Arhgef2 (pS940/pT944), Ralgapa1 (pS859) and Sipa1l1 (pS1534/pS1544/pS1547), as well as actin-binding proteins such as Afap1 (pS669), spinophilin (pS100) (also known as Ppp1r9b), Marcks (pS163) and moesin (pS384). We found that 53 sites in 46 proteins were phosphorylated only in the presence of wild-type talin (Table S4), with the most enriched GO term being 'regulation of cell migration' (Table S5). Accordingly, these proteins include adhesion signaling proteins, such as vinculin (pS290), zyxin (pS269/pS272), p190RhoGAP (pS975), insulin receptor substrate 1 (pT525/pS526), reticulon-4 (pS223), MAP3K1 (pS142) and misshapen-like kinase 1 (pS603). Conversely, 169 sites in 138 proteins were phosphorylated in all samples except cells expressing wild-type talin. These proteins include regulators of the actin cytoskeleton, such as Ena/VASP like-protein Evl (pS329), TRIO-binding protein (pS1591), Rho GTPase-activating protein 18 (pS63/pS64), Rho guanine nucleotide exchange factor 5 (pS782) and myosin phosphatase Rho-interacting protein (pT540), as well as signaling proteins including protein kinase Cδ (pS504/pT505), cAMP-dependent protein kinase catalytic subunit beta (pT198) and A-kinase anchor protein 2 (pS740).

As some of the signaling pathways activated by the talin rod domain may have basal activity in the absence of talin proteins, we also analyzed the same data by quantitative pairwise analysis using 5-fold enrichment as a cutoff (Fig. 3B; Tables S6 and S7). Again, we identified differential phosphorylation in a number of proteins associated with the regulation of either Rho-family GTPases or actin polymerization and bundling (Fig. 3B). Of the identified GTPase regulators, the interaction network containing p190RhoGAP and its regulators p120Cas and paxillin was differently phosphorylated in all compared pairs, suggesting that both the transmission of mechanical forces and the transduction of these forces by talin rod domain contribute to the regulation of this pathway. To investigate the roles of talin rod domain mechanotransmission and mechanotransduction in the regulation of phosphotyrosine signaling and RhoA activity, we selected the FAK–paxillin–p190RhoGAP signaling module and the adhesion adapter protein p130Cas for further analysis by confocal microscopy.

Talin mechanotransmission activates phosphotyrosine signaling in the absence of talin rod mechanotransduction

In non-transfected *Tln1*$^{-/-}$*Tln2*$^{-/-}$ cells, immunostaining of activated (pY397) FAK revealed punctuate activation at the points of cell–substrate contacts (Fig. 4A). Similar intense, but punctuate, foci of FAK activation were observed at the front of the band of adhesions in cells expressing talin head domain (Fig. 4A,B). However, these sites of FAK activation did not colocalize with the talin head domain, suggesting that other factors, such as kindlin-2 and paxillin (Theodosiou et al., 2016), mostly account for the recruitment and activation of FAK in these cells. In contrast to talin head domain, expression of the talin ΔR1-12 facilitated the recruitment of activated FAK into adhesion sites (Fig. 4B,C), indicating that talin mechanotransmission indeed contributes to the regulation of phosphotyrosine signaling independently of talin rod mechanotransduction. This increase was also seen after normalizing the FAK pY397 intensity to the intensity of talin itself (Fig. 4D), confirming that the observed FAK activation was not merely reflecting the level of the ΔR1-12 protein adhesion recruitment. In line with immunofluorescence, western blot analysis supported the finding of increased FAK Y397 phosphorylation in ΔR1-12 -expressing cells compared to cells expressing talin head domain (Fig. S4A).

Interestingly, the subcellular sites enriched with activated FAK only partially colocalized with the ΔR1-12 protein. This suggests that talin rod subdomains R1-12 and their mechanical activation are likely required for the correct spatial regulation of adhesion complex nanoscale structure and FAK-substrate interactions. Expression of any of the three talin proteins containing mechanosensitive rod subdomains (ΔR10-12, ΔR4-12 and wild-type talin) resulted in a further increase in adhesion FAK pY397 intensity (Fig. 4C,D). To confirm that the talin rod-mediated increase in FAK activation was dependent on the mechanical activation of the talin rod domain, we analyzed FAK activation in cells expressing the ΔR1-12+C-terminal R1-3 talin protein. As expected, this reorganized talin was unable to induce FAK activation beyond the level achieved with the ΔR1-12 protein, demonstrating that mechanical activation of the talin rod subdomains is required for their functionality in the regulation of FAK recruitment and activity (Fig. S4B–D). Although the destabilization of the talin rod R3 subdomain resulted in an increase in the absolute level of FAK pY397 (Fig. S4E,F), it decreased the talin/pY397 ratio (Fig. S4G). Similarly, although the R1-3 subdomain fragments in tandem configuration increased the vinculin/talin ratio (Fig. 2O), this increase was not reflected in the pY397/talin ratio. Taken together, these results indicate that, while the mechanical activation of talin rod subdomains is required for full FAK activity, the talin-mediated recruitment of vinculin is not alone sufficient for increased FAK activity.

To investigate whether the observed talin-mediated activation of FAK is further reflected in the activation of other signaling proteins, we analyzed the localization and activation of the well-known downstream targets of FAK: paxillin, p130Cas and p190RhoGAP (Arthur and Burridge, 2001; Tsubouchi et al., 2002). As seen for FAK, the absolute intensities of activated paxillin (pY31) and activated p130Cas (pY410) were higher in cells expressing the ΔR1-12 protein compared to talin head-expressing cells (Fig. 4E,G; Fig. S4H,I). However, this increase in paxillin and p130Cas activity was not seen after normalization to talin intensity (Fig. 4F,H). This indicates that the increased activation of FAK by the ΔR1-12 protein is not directly reflected in the phosphorylation status of the other phosphotyrosine signaling proteins within the adhesion.

p190RhoGAP is a major negative regulator of RhoA, and its FAK-dependent activation by Y1105 phosphorylation is required for the local inhibition of myosin activity in cell lamellipodia (Arthur et al., 2000; Arthur and Burridge, 2001). Staining of activated (pS19) myosin light chain-2 (MLC2) revealed a differential regulation of myosin activity in cells expressing the ΔR1-12 protein compared to talin forms capable of talin rod unfolding. In the cells expressing the ΔR1-12 protein, the region of activated MLC2 extended all the way to the leading edge of the cell lamellipodium (Fig. 4I–K). In contrast, the expression of either ΔR4-12 or wild-type talin resulted in the formation of a distinct zone lacking MLC2 activity at the front part of lamellipodia. This finding is in line with the lack of paxillin and p130Cas activation in the cells expressing ΔR1-12 protein, and suggests that, while talin mechanotransmission contributes to the activation of FAK in adhesion sites, further force- and talin rod-dependent activation of adhesion signaling proteins is required for the normal regulation of adhesion phosphotyrosine signaling.

The presence of talin rod subdomains and their correct mechanical stability are required for the recruitment of the actin regulatory protein VASP

As the transmission of mechanical force through talin forms was found to mediate the recruitment and activation of some adhesion

Journal of Cell Science (2019) 132, jcs226514. doi:10.1242/jcs.226514

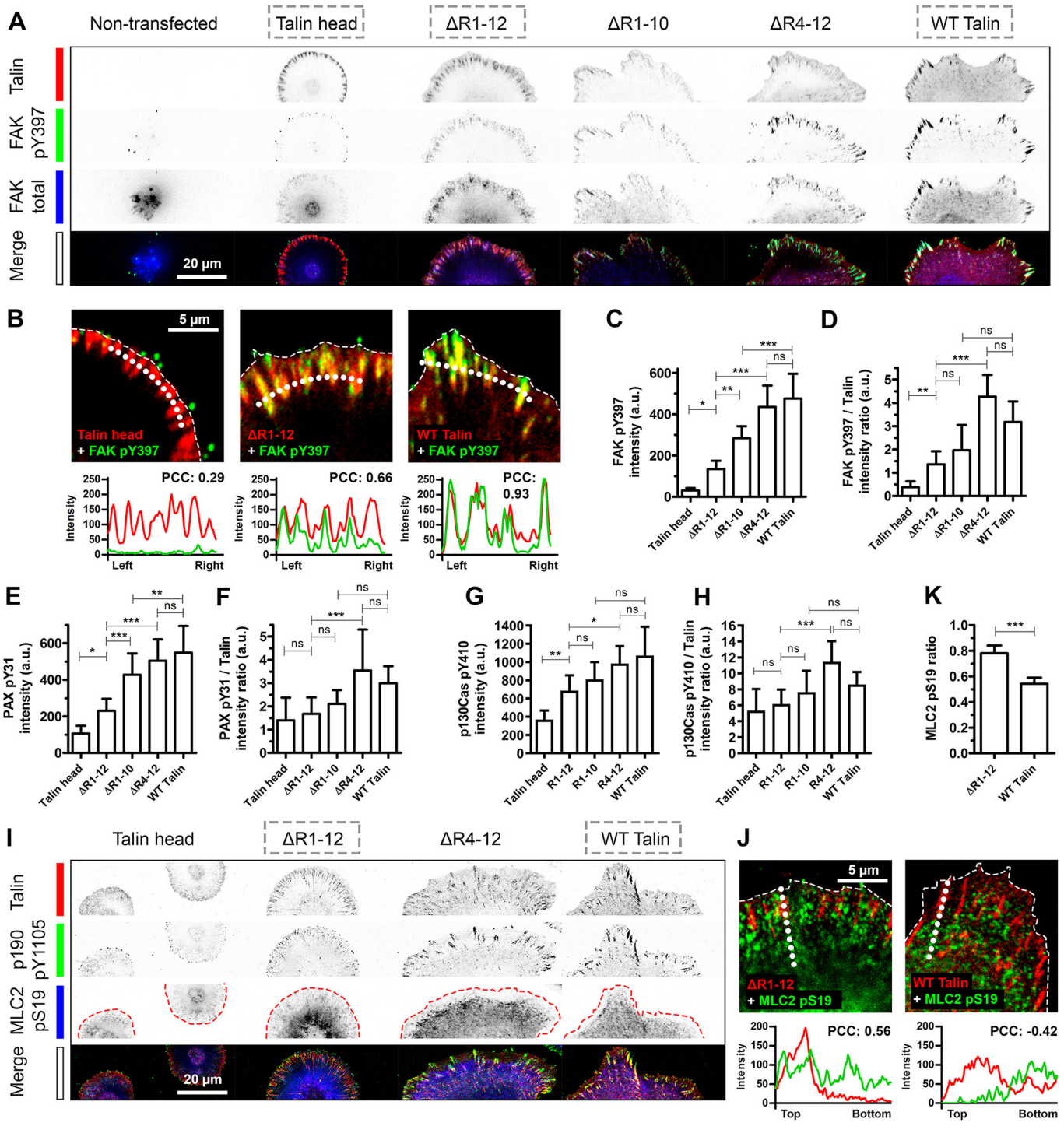

Fig. 4. Talin mechanotransmission activates phosphotyrosine signaling independently of talin rod mechanotransduction. (A) Representative images of total FAK and FAK pY397 (activated) immunostaining. (B) Close-ups of the samples marked with dashed line boxes in A. Intensities of talin and FAK pY397 were measured along 12-μm selections (dotted lines) perpendicular to cell–matrix adhesions and plotted as line graphs (below). Note how Y397 phosphorylated FAK is not colocalized with the talin head domain and only partially colocalized with the ΔR1-12 protein. (C) Fluorescence intensity analysis for adhesion localized pY379 FAK. *n*=14–28 cells pooled from two independent experiments. (D) FAK pY397 intensity in C normalized to the average talin adhesion intensity in each cell. (E,F) Fluorescence intensity analysis for adhesion-localized paxillin pY31 and talin-normalized pY31 intensity. *n*=14–19 cells pooled from two independent experiments. (G,H) Intensity analysis for adhesion-localized p130Cas pY410 and talin-normalized pY410 intensity. *n*=10–11 cells for each talin protein. (I) Representative images of p190RhoGAP pY1105 and MLC2 pS19 immunostaining. Red dashed lines indicate the edge of the cell lamellipodium. (J) Close-ups of the samples marked with dashed line boxes in I. Intensities of talin and MLC2 pS19 were measured along 10-μm selections (dotted lines) parallel to the cell–matrix adhesions. In B and J, the dashed white lines indicate the cell edge. (K) Lamellipodium/lamella ratio for the average MLC2 pS19 intensity within 5 μm from the cell front (lamellipodium) and elsewhere in the cytosol (lamella). *n*=12 and 15 cells for ΔR1-12 and WT, respectively. Data are mean±s.d. The statistical significance of all results was analyzed by one-way ANOVA and Bonferroni test. ns, not significant; **P*<0.05, ***P*<0.01, ****P*<0.001.

Journal of Cell Science

Journal of Cell Science (2019) 132, jcs226514. doi:10.1242/jcs.226514

proteins even in the absence of talin rod subdomains, we were curious to see whether this effect was reflected in the recruitment of proteins regulating actin polymerization and bundling. The actin regulatory protein VASP is recruited to adhesion complexes by FPPPP-motif proteins such as vinculin, zyxin and mDia2 (also known as Diaph3). As expected, both ΔR4-12 and wild-type talin facilitated robust recruitment of VASP into adhesion sites (Fig. 5A, B,D). In contrast, in cells expressing talin head, ΔR1-12 or ΔR1-12+C-terminal R1-3 (data not shown), VASP strongly localized to the edge of the circular lamellipodium and was completely absent from adhesion sites (Fig. 5A,B). This indicates that both the presence and the mechanical activation of talin rod subdomains are required for the recruitment of VASP into the adhesion complex. To investigate whether the lack of VASP recruitment to adhesion sites could be rescued by forced recruitment of the FPPPP protein vinculin, we created a fusion construct composed of talin head domain and full-length vinculin. Although this fusion protein facilitated cell spreading similarly to the ΔR1-12 talin form, it did not recruit VASP into the adhesion complex (Fig. S5). Similar results were seen for the fusion of talin head to the autoinhibition-deficient vinculin T12 mutant, indicating that the lack of VASP recruitment by talin head–vinculin fusion protein is not caused by the autoinhibited conformation of vinculin (Fig. S5). Surprisingly, loss of VASP recruitment was also observed for the destabilized ΔR4-12 (4S) protein (Fig. 5A,C–E) despite the strong recruitment of vinculin by this talin form (Fig. 2N). Again, the lack of VASP recruitment could be rescued by the addition of one or two intact R1-3 fragments into the destabilized talin protein (data not shown). These results indicate that, although talin-bound vinculin is known to mediate the recruitment of VASP (Brindle et al., 1996; Hüttelmaier et al., 1998), other factors additional to vinculin are required for the correct regulation of VASP recruitment. Such factors may include sufficient mechanical tension in the actin cytoskeleton or the presence of multiple FPPPP proteins in the correct nanoscale organization.

DISCUSSION

Talin functions both as a structural linkage and as a signaling protein in adhesion complexes. However, the contributions of talin rod domain mechanotransduction and its structural mechanotransmission in adhesion reinforcement and signaling have remained unknown. Here, our aim was to dissect the roles of talin mechanotransmission and mechanotransduction in the regulation of adhesion dynamics, protein composition and signaling activity by expressing modified talin proteins in talin-null cells. We demonstrate that the mechanical coupling of integrins and actin by talin contributes to the stabilization of adhesion sites and initializes phosphotyrosine signaling events in the absence of talin rod subdomains R1-12. Furthermore, utilizing proximity proteomics, we demonstrated that the transmission of mechanical force through talin regulates the recruitment of various proteins independently of talin rod unfolding. These proteins included known talin partners, poorly understood adhesion proteins as well as multiple regulators of phosphotyrosine signaling. The presence and mechanical activation of talin rod domains was found to

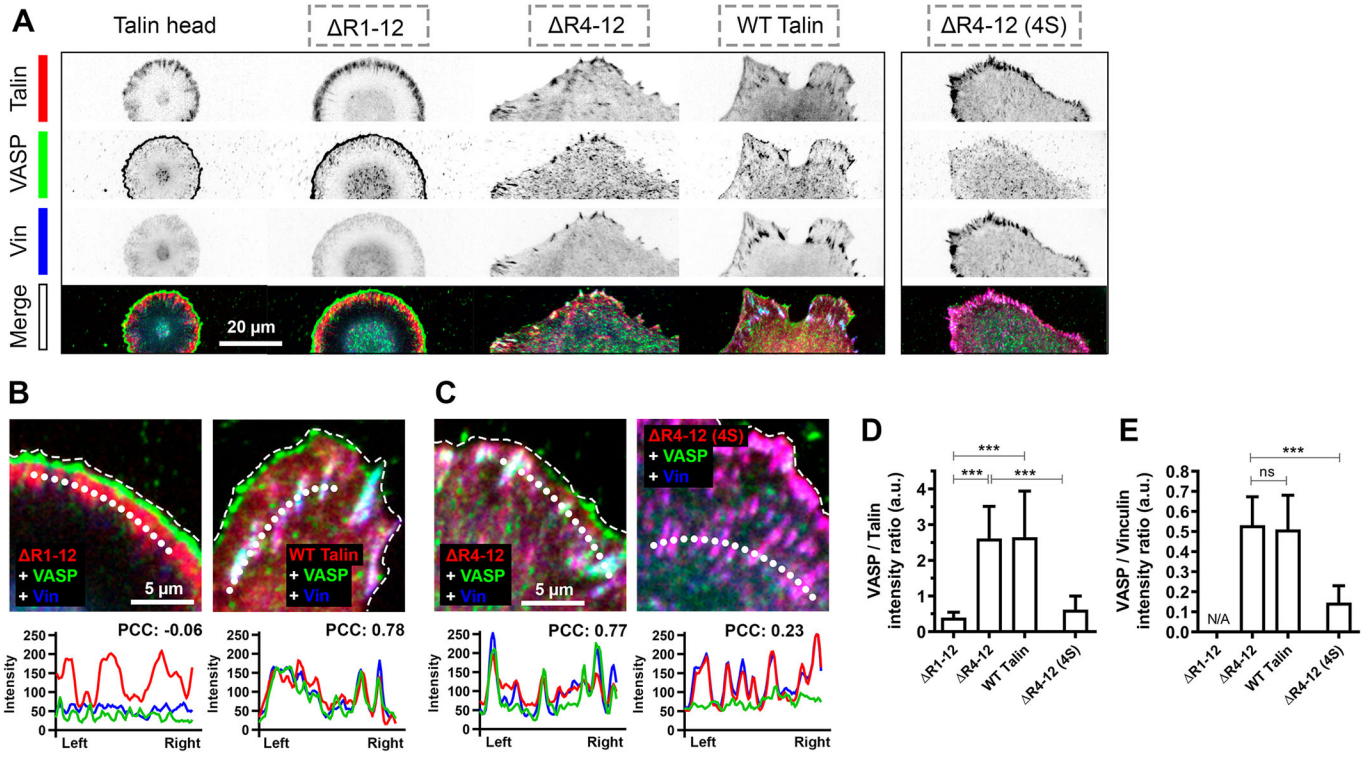

Fig. 5. The presence of talin rod subdomains and their correct mechanical stability are required for the recruitment of actin regulatory protein VASP. (A) Representative images of cells stained with an anti-VASP and anti-vinculin antibodies. Note how VASP is localized to the leading edge of lamellipodium in cells expressing ΔR1-12, while the expression of ΔR4-12 or WT talin allows VASP recruitment into adhesion sites. (B,C) Comparison of VASP colocalization with ΔR1-12 and WT talin or ΔR4-12 and ΔR4-12 (4S), respectively. Intensities of talin and VASP were measured along 15-μm selections (dotted lines) and plotted as line graphs (below). PCC, Pearson correlation coefficient for talin and VASP. The dashed white lines indicate the cell edge. (D,E) VASP/talin and VASP/vinculin intensity ratios for adhesion sites. *n*=12, 10, 12 and 10 cells for ΔR1-12, ΔR4-12, WT talin and ΔR4-12 (4S), respectively. The low level of vinculin and VASP colocalization with ΔR1-12 prevented reliable analysis of the VASP/vinculin ratio for this talin protein. The statistical significance of all results was analyzed by one-way ANOVA with Bonferroni test. ns, not significant; ***P<0.001.

be indispensable for adhesion reinforcement, traction force generation and cell migration. Experiments utilizing excessively active destabilized talin proteins demonstrated that the talin rod subdomains and their fine-tuned mechanical properties are critical for the generation of cellular signaling anisotropy and establishment of cell polarity. Interestingly, the talin rod domain was also found to be required for the recruitment of the tumor suppressor protein testin, suggesting that it may act as a novel effector protein downstream of the force-regulated unfolding of talin rod subdomains.

Talin mechanotransmission contributes to adhesion stability and signaling but cannot trigger adhesion reinforcement in the absence of rod subdomains R1-12

Adhesion complex reinforcement as a response to mechanical forces is mediated by both the recruitment of structural adhesion proteins such as vinculin and by the activation of downstream signaling cascades. However, as exemplified by the ΔR1-12 protein, the transmission of mechanical forces through the talin protein regulates adhesion dynamics independently of talin rod domain. This force-dependent, but talin rod domain-independent, modulation of adhesion dynamics is likely attributed to the multiple catch-bond interactions between force-bearing adhesion proteins, as well as to other tension-dependent processes, such as the force-regulated exposure of cryptic interaction sites in fibronectin molecules (Guo and Guilford, 2006; Kong et al., 2009; Hayakawa et al., 2011; Hytönen and Wehrle-Haller, 2016; Benito-Jardón et al., 2017; Huang et al., 2017). Accordingly, the ΔR1-12 protein was found to decrease the rate of actin retrograde flow in lamellipodia compared to talin head domain and to mediate the reorganization of fibronectin molecules. This indicates that the mechanical connection through the ΔR1-12 protein can transiently resist the traction forces generated by the actin retrograde flow in cell lamellipodia. The experiments with talin ΔR13-DD also confirmed the importance of ABS3 in cell polarization (Fig. 2E–G) and cell migration (Fig. 2H). However, similarly to the previously characterized vinculin-deficient cells (Thievessen et al., 2013), cells expressing the ΔR1-12 protein lacked a clear lamellipodia–lamella border. This indicates that the talin rod- and vinculin-dependent reinforcement of the adhesion complex is required for the formation of mature adhesions able to resist the high-magnitude forces generated by actomyosin contraction.

The results of the study demonstrated that, while the ΔR1-12 protein activates FAK autophosphorylation, the presence of talin rod subdomains is required for full FAK activity. This talin rod-dependent FAK activation could be mediated by the talin–vinculin–paxillin–FAK (Subauste et al., 2004) or talin–DLC1–paxillin–FAK (Zacharchenko et al., 2016; Haining et al., 2018) signaling modules. The ΔR1-12 protein, however, cannot directly interact with vinculin, paxillin or DLC1. Thus, the mechanisms mediating the increased FAK activation in cells expressing this construct must be independent of these proteins. Interestingly, experiments with a FAK biosensor have suggested that mechanical loading of fibronectin–α5β1 interaction activates FAK through the increased clustering of integrins and FAK (Seong et al., 2013). As the interaction of the FAT domain in FAK with talin head is not required for the integrin-mediated activation of FAK (Lawson et al., 2012), it seems that, especially in nascent adhesions, talin regulates FAK activity through the mechanical and biochemical activation of integrins. However, in mature adhesions, the talin rod-dependent mechanisms seem to be critical for the increased FAK activity and correct regulation of various adhesion functions. In addition to these mechanisms, recent molecular dynamics simulations suggest that mechanical force may also directly activate membrane-bound FAK (Zhou et al., 2015; Bell and Terentjev, 2017). However, biochemical evidence of this mechanism and understanding of the role of talin and other FAT domain-binding proteins in it are still lacking. Taken together, these findings indicate that the level of adhesion phosphotyrosine signaling is regulated by multiple talin-dependent mechanisms. While the complete activation of FAK signaling is dependent on the mechanical regulation of the talin rod domain, the results of this study demonstrate that talin rod-independent mechanisms also contribute to the overall level of FAK activity.

Why is the FAK Y397 phosphorylation in cells expressing talin ΔR1-12 not translated into the phosphorylation of FAK substrates p130Cas and paxillin? We could speculate that this is associated with poor ‘substrate presentation’, i.e. the adhesion nanoscale structure is affected in the absence of mechanoregulated talin rod subdomains, leading to a decrease in interactions between FAK and its natural substrates. For example, previous studies have shown that paxillin interacts with talin head domain (Gao et al., 2017), but there are numerous other binding partners for paxillin in the focal adhesions, many of which are mechanoregulated (Hytönen and Wehrle-Haller, 2014). Therefore, the differences in paxillin and FAK phosphorylation levels could be associated with the absence of vinculin recruitment to adhesions established on talin ΔR1-12, leading to compromised positioning of paxillin in relation to FAK and reflected in decreased paxillin Y31 phosphorylation rate. Overall, this model emphasizes the importance of the scaffolding function of talin.

Similarly, the recruitment of actin regulator VASP was found to be fully dependent on both the presence and correct mechanical regulation of the talin rod subdomains. As both ΔR1-12 and ΔR4-12 (4S) proteins were unable to recruit VASP, it seems that mechanisms other than the talin rod-dependent recruitment of FPPPP proteins such as vinculin must regulate the recruitment of VASP into adhesion sites. Whether these mechanisms are dependent on the phosphorylation of VASP or FPPPP proteins or on the correct level of mechanical tension in the actin cytoskeleton will be an interesting subject for future studies.

Talin rod domain mechanosensing is a robust process mediated by multiple parallel mechanisms

The finding that both ΔR1-10 and ΔR4-12 proteins can mediate adhesion complex reinforcement and signaling indicates that none of the talin rod subdomains is critically required for these processes. Both the ΔR1-10 and ΔR4-12 proteins each contain only a limited set of the mechanosensitive rod subdomains (R1-3 and R10-12, respectively) and lack most of the interaction sites for other adhesion proteins (e.g. actin, vinculin, RIAM, DLC1, α-synemin, Kank1 and Kank2). Nevertheless, the mechanically regulated interactions of the subdomains R1-3 or R11-12 are sufficient to mediate the force-dependent reinforcement of adhesions *in vitro*, as indicated by cell polarization and migration. These rod subdomains contain mechanically regulated binding sites for both vinculin (rod subdomains R1, R2, R3, R12, R13) and RIAM (R2-3, R8, R11), interacting with a large number of adhesion proteins. Both vinculin and RIAM can directly regulate actin polymerization (through Ena/VASP proteins and Arp2/3 complex) and phosphotyrosine signaling (through paxillin and PLCγ). Accordingly, expression of both vinculin and RIAM has been shown to be required for normal adhesion structure and function (Lafuente et al., 2004; Thievessen et al., 2015), and overwhelming evidence demonstrates the importance of vinculin in adhesion mechanosensing and reinforcement (Carisey et al., 2013; Thievessen et al., 2013, 2015; Elosegui-Artola et al., 2016). However, experiments with vinculin

Journal of Cell Science (2019) 132, jcs226514. doi:10.1242/jcs.226514

and RIAM knockout cell lines have unambiguously demonstrated that neither vinculin nor RIAM is required for the force-regulated reinforcement of the adhesion structure (Coll et al., 1995; Xu and Baribault, 1998; Lafuente et al., 2004). In addition, vinculin was found to be dispensable for the nanoscale organization of adhesion complexes (Thievessen et al., 2013; Liu et al., 2015). Therefore, it seems that many partially redundant structural (e.g. through the binding of actin filaments) and signaling (e.g. through the recruitment of signaling proteins) mechanisms contribute to the talin rod-dependent reinforcement and signaling of adhesion complexes. Although other integrin and actin-binding proteins, such as α-actinin, filamin-A and tensin, may contribute to the force-regulated reinforcement of the adhesion complex, especially during the early phases of its formation (Glogauer et al., 1998; Ye et al., 2014; Meacci et al., 2016; Wolfenson et al., 2016), the results presented here indicate that the talin rod subdomains are indispensable for the complete reinforcement and maturation of focal adhesions.

Talin rod domain mechanotransduction is required for the generation of cellular signaling anisotropy

While the mechanical activation of talin rod domain was found critical for cell polarization, its excessive activation by destabilization abolished cell polarity. The concurrent increase in the recruitment of talin, vinculin and activated FAK in the cells expressing the destabilized proteins suggests that talin destabilization prevented the correct spatial regulation of adhesion signaling activity. Although the gradual, force-regulated activation of the talin rod domain normally generates spatial differences in the level of adhesion signaling, the destabilized ΔR4-12 (4S) talin form is likely readily activated by low-magnitude forces throughout the cell. This results in the loss of cellular signaling anisotropy and prevents the establishment of cell polarity. Accordingly, talin proteins with additional R1-3 rod fragments were able to rescue cell polarity and cell migration (Fig. 2I,L). Although these proteins contain the same destabilized R3 subdomain, the additional rod subdomains present in these proteins are only activated by sufficient mechanical tension, restoring the signaling anisotropy. This is demonstrated by the observed further increase in the recruitment of vinculin in cells expressing tandem proteins. Based on the results presented here, we propose that the correct, spatially restricted mechanical activation of talin rod domain is required for the establishment of cell polarity in many adherent cell types.

Taken together, the results of this study demonstrate that both talin rod domain mechanotransmission and mechanotransduction contribute to the regulation of adhesion dynamics and to the activation of adhesion signaling. However, adhesion reinforcement, cell polarization and cell migration were found to be dependent on the mechanical regulation of the talin rod domain. Importantly, the results presented here indicate that talin rod domain mechanosensing is mediated by multiple, interlinked mechanisms that regulate adhesion reinforcement and downstream signaling through different pathways. Dissection of the talin rod-dependent and rod-independent mechanisms mediating the force-regulated adhesion reinforcement and signaling presents an intriguing challenge for future studies. The results of proximity scanning proteomics provide potential candidate proteins to explore the interactions involved in these processes.

MATERIALS AND METHODS

Experimental model

The *Tln1*$^{-/-}$*Tln2*$^{-/-}$ mouse embryonic fibroblast (MEF) cell line used in this study has previously been described by Theodosiou et al. (2016). Cells were maintained in high-glucose Dulbecco's modified Eagle medium (DMEM) supplemented with 10% fetal bovine serum and 1% GlutaMax (Thermo Fisher Scientific) in a humidified 37°C, 5% CO_2 incubator. The cell line was regularly tested (~1-month intervals) for mycoplasma contamination.

Expression constructs and cell transfection

EGFP- or mCherry-tagged talin-1 and vinculin expression constructs were created by subcloning of complementary DNA (cDNA) fragments encoding mouse talin-1, vinculin or EGFP/mCherry fluorescent proteins into a modified pEGFP-C1 vector backbone (Clontech). BioID expression constructs were created by Gateway cloning cDNA fragments encoding different talin proteins into the previously described MAC-tag vector (Liu et al., 2018). The structures of the modified talin and vinculin constructs are presented below. All plasmid constructs were authenticated by sequencing. *Tln1*$^{-/-}$*Tln2*$^{-/-}$ MEF cells were transfected with the Neon transfection system (Thermo Fisher Scientific). For all plasmid constructs, 5 µg plasmid DNA and the electroporation parameters 1400 V, 30 ms, one pulse were used per 10^6 cells.

The expression constructs were as follows: wild-type talin, 1-2541+mCherry or EGFP+1-2541; talin head, mCherry/EGFP+1-490; ΔR1-12, 1-490+2296-2541+mCherry/EGFP; ΔR1-12+C-terminal R1-3, 1-490+2296-2541+487-913+mCherry; ΔR1-10, 1-490+1974-2541+mCherry/EGFP; ΔR13-DD, 1-2300+GlyGlySerGly linker+EGFP; ΔR4-12, 1-913+2296-2541+mCherry/EGFP; ΔR4-12 (4S), 1-913+2296-2541 (I805S, I812S, L890S, L897S)+mCherry/EGFP; ΔR4-12 (4S)+R1-3, 1-913 (I805S, I812S, L890S, L897S)+487-913+2296-2541+mCherry; ΔR4-12 (4S)+2x R1-3, 1-913 (I805S, I812S, L890S, L897S)+2x 487-913+2296-2541+mCherry; vinculin, EGFP+vinculin 1-1066; vinculin (T12), EGFP+vinculin 1-1066 (D974A, K975A, R976A, R978A); vinculin head, EGFP+vinculin 1-255; talin head+vinculin fusion, EGFP+talin 1-490+vinculin 1-1066; talin head+vinculin fusion (T12), EGFP+talin 1-490+vinculin 1-1066 (D974A, K975A, R976A, R978A); talin proteins+BirA, talin proteins with C-terminal BirA R118G mutant.

Immunostaining and confocal imaging

Zeiss high-performance 170-µm-thick coverslips were washed with 2% Hellmanex-III (Merck) in a bath sonicator at 40°C for 20 min (Finnsonic), rinsed with water and attached to perforated 35-mm polystyrene dishes (MatTek, Ashland, MA). The coverslips were coated with 25 µg/ml human fibronectin for 1 h at 37°C and washed twice with PBS. *Tln1*$^{-/-}$*Tln2*$^{-/-}$ MEF cells were transfected with talin expression constructs and allowed to recover for 24 h. The transfected cells were trypsinized and plated at low confluency on fibronectin-coated coverslips for 120 min, after which the medium was aspirated from the wells and the cells fixed with 4% paraformaldehyde (PFA) in PBS (pH 7.4) for 15 min at room temperature (RT). The fixed cells were washed twice with PBS and permeabilized with 0.2% Triton X-100 in PBS for 5 min at RT. Non-specific antibody binding was blocked by incubating the samples in 5% fetal calf serum, 1% bovine serum albumin (BSA) and 0.05% Triton X-100 in PBS for 30 min at RT.

The following antibodies and dilutions were used: anti-vinculin antibody (Merck, clone hVIN-1, V9131, RRID:AB_477629), 1:400; anti-paxillin (BD Biosciences, 349/Paxillin, 610051, RRID:AB_397463), 1:100; anti-paxillin-pY31 (Thermo Fisher Scientific, 44-720G, RRID:AB_1501920), 1:200; anti-FAK (BD Biosciences, 77/FAK, 610088, RRID:AB_397495), 1:100; anti-FAK-pY397 (Abcam, ab81298 [EP2160Y], RRID:AB_1640500), 1:200; anti-p190RhoGAP-pY1105 (Merck, SAB4503875), 1:100; anti-VASP (Merck, HPA005724, RRID:AB_1858721), 1:100; anti-MLC2-pS19 (Cell Signaling Technology, 3675, RRID:AB_2147461), 1:200; and anti-testin (Atlas Antibodies HPA018123, RRID:AB_1857900), 1:200. Alexa Fluor 488-, 568- and 633-conjugated anti-mouse and anti-rabbit antibodies diluted 1:250 into the blocking buffer were used as secondary antibodies (Thermo Fisher Scientific). After each step, immunostained coverslips were washed with PBS (3×10 min). Immunostained samples were stored at +4°C until imaged.

For colocalization analysis, immunostained samples were imaged with a Nikon Eclipse Ti inverted microscope (Nikon Instruments) equipped with a CFI Plan Apo VC 60×/1.40 NA oil immersion objective (Nikon Instruments), a CSU10 spinning disk confocal unit (Yokogawa, Tokyo, Japan) and an Andor NEO sCMOS camera (Andor Technology). Then,

Journal of Cell Science (2019) 132, jcs226514. doi:10.1242/jcs.226514

488 nm, 561 nm and 640 nm lasers were used to excite fluorescent GFP and mCherry proteins or Alexa Fluor 488, 568 and 633 fluorophores, respectively. The imaging parameters were kept constant for all samples within each experiment to allow quantitative image analysis. For the quantification of adhesion-localized protein intensity in single cells, 8–15 adhesion sites with the highest intensity on the talin channel were selected using circular selections (diameter 0.7 µm). Selections were made on the *Z*-plane with the best contrast and copied to the matching plane of the other fluorescence channels. For background correction of adhesion intensity, the intensities of five circular areas (diameter 2.2 µm) immediately next to the analyzed adhesion sites were measured.

For the analyses of cell area and polarization, PFA-fixed cells were stained with phalloidin and imaged with a Zeiss CellObserver.Z1 equipped with a 25×/0.8 NA oil immersion objective and a LSM780 confocal unit (Zeiss, Oberkochen, Germany). Zeiss Zen Black software and ImageJ 1.50e were used for image analysis (Schneider et al., 2012).

Western blotting

For FAK pY397 analysis, transfected *Tln1*$^{-/-}$*Tln2*$^{-/-}$ cells were grown for 48 h post-transfection. Cells were then detached using TrypLE (Gibco), after which trypsin was briefly inactivated with serum-containing medium. Suspension cells were plated on plastic well plates with full serum growth medium. After indicated time points, cells were washed twice with PBS and collected to Laemmli SDS sample buffer. After SDS–PAGE and blotting onto polyvinylidene fluoride membrane, membranes were immunostained with antibodies against FAK pY397 (see above) and actin (Millipore, MAB 1501R, RRID:AB_2223041). Appropriate secondary antibodies (LI-COR) and a LI-COR imaging system were used to detect bound primary antibodies. Phospho-FAK (pFAK) and actin antibody intensities were analyzed using image studio Lite, and pFAK values were normalized against actin intensities.

Migration analysis

Polystyrene well plates were coated with 10 µg/ml fibronectin at 37°C for 1 h and washed twice with PBS (pH 7.4). Transfected *Tln1*$^{-/-}$*Tln2*$^{-/-}$ MEF cells were allowed to recover for 24 h, trypsinized and plated onto fibronectin-coated well plates at a low confluency. Cells were allowed to attach for 1 h, followed by a wash with warm PBS (pH 7.4) to remove dead or non-transfected cells. Cells were incubated in fresh medium for 30 min before the imaging. The EVOS FL Auto microscope (Thermo Fisher Scientific) equipped with a 37°C and 5% CO_2 incubator was used for live-cell imaging for 12 h at 120- or 360-s intervals. The resulting image stacks were analyzed with ImageJ version 1.50e (Schneider et al., 2012) and MTrackJ plugin (Meijering et al., 2012).

Collagen-I matrix contraction assay

For the collagen-I matrix contraction assay, ring-shaped polydimethylsiloxane (PDMS) casts placed at the bottom of six-well plate wells were coated with 1% BSA in PBS for 1 h at 37°C, washed twice with PBS, air-dried and sterilized by a UV light source. Transfected *Tln1*$^{-/-}$*Tln2*$^{-/-}$ cells were cultured for 24 h post-transfection, trypsinized and counted. The number of cells in the complete polymerized collagen-I matrix was 312,000 cells per 100 µl of the matrix mixture. Cells were resuspended in DMEM in one-third of the final volume of the mixture, while the rest of the mixture was composed of the following components: 1/10 of 10× DMEM, 1/10 of 0.5 M NaOH and 8/10 of 3 mg/ml rat tail collagen-I (Thermo Fisher Scientific, A1048301). All components were carefully mixed on ice and the matrix mixture was casted into the BSA-coated PDMS wells. The collagen-I matrixes were allowed to polymerize for 30 min at 37°C, after which the PDMS casts were released and the wells filled with warm complete medium. The macroscopic contraction of the collagen-I matrices was followed at 24 h intervals for 72 h by a gel imager.

FRAP

For FRAP analysis, *Tln1*$^{-/-}$*Tln2*$^{-/-}$ cells were transfected with C-terminally GFP-tagged talin proteins. Transfected cells were allowed to recover for 24 h and plated on fibronectin-coated (25 µg/ml) glass-bottom dishes 2 h before imaging. A Zeiss Cell Observer.Z1 microscope equipped with an LSM780 confocal unit, 37°C/5% CO_2 incubator and 63×/1.4 NA oil immersion objective was used for imaging. One circular region per cell with a diameter of 2.6 µm was photobleached with a 488 nm argon laser operated at a high intensity. Confocal microscope images were captured at 1-s intervals for 5 s before photobleaching and for 90 s after photobleaching. The results were pooled from two independent experiments. Fluorescence recovery was analyzed by the equation F=[B(t)/B(t<0)]/[Cell(t)/Cell(t<0)], where B(t<0) and Cell(t<0) are the average fluorescence intensities of the of bleached area and the entire cell, respectively, before bleaching and B(t) and Cell(t) intensities of the same regions at each time point after bleaching. EasyFRAP software was used for the fitting single exponential curves to each series individually to calculate mobile fraction and half-recovery times for each region (Rapsomaniki et al., 2012).

Lysate preparation and tandem MS (MS/MS) analysis

For the BioID analysis, *Tln1*$^{-/-}$*Tln2*$^{-/-}$ cells were transfected with Jetpei reagent (Polyplus transfections) according to the manufacturer's instructions and cultured for 24 h. Transfected cells were detached and divided into six 15-cm culture plates. After 24 h, 50 µM biotin was added to the culture medium for 24 h. Cells were washed, collected, snap frozen and lysed on ice in HENN lysis buffer (50 mM HEPES pH 8.0, 5 mM EDTA, 150 mM NaCl, 50 mM NaF, supplemented with 0.5% NP-40, 0.1% SDS, 1 mM DTT, 1.5 mM Na_3VO_4, 1 mM PMSF and 1× protease inhibitor cocktail; Sigma-Aldrich). Cleared lysates were loaded on spin columns (Bio-Rad) containing 200 ml Strep-Tactin beads (IBA), washed three times with washing buffer (HENN+0.5% NP-40, 1 mM DTT, 1.5 mM Na_3VO_4, 1 mM PMSF and 1× protease inhibitor cocktail) and then washed four times with HENN buffer. Bound proteins were eluted with 2×300 µl freshly prepared 0.5 mM D-biotin (Thermo Fisher Scientific) in HENN buffer. The samples were reduced with 5 mM Tris(2-carboxyethyl)phosphine (TCEP) and alkylated for cysteine bonds with 10 mM iodoacetamide. The sample proteins were digested with trypsin (Promega) overnight at 37°C and tryptic peptides were purified using C18 microspin columns (The Nest Group).

Liquid chromatography (LC)-MS/MS analysis was performed with a Q Exactive ESI-quadrupole-orbitrap mass spectrometer coupled to an EASY-nLC 1000 nanoflow LC (Thermo Fisher Scientific), using Xcalibur version 3.1.66.10 (Thermo Fisher Scientific), as previously described (Liu et al., 2018). For each sample, three technical replicates were loaded into a C18-packed precolumn (Acclaim PepMap™100, 75 µm×2 cm, 3 µm, 100 Å, Thermo Fisher Scientific). Peptides were separated using a C18-packed analytical column (Acclaim PepMap™RSLC, 75 µm×15 cm, 2 µm, 100 Å, Thermo Fisher Scientific) with a 60-min linear gradient from 5% to 35% of buffer B [98% acetonitrile (ACN) and 0.1% formic acid] at a flow rate of 300 nl/min. The mass spectrometry analysis was performed in data-dependent acquisition in positive-ion mode. MS spectra were acquired from m/z 200 to m/z 2000 with a resolution of 70,000, with a full automatic gain control (AGC) target value of 1,000,000 ions and a maximal injection time of 100 ms, in profile mode. The ten most abundant ions of which charge states were 2+ to 7+ were selected for subsequent fragmentation [higher-energy collisional dissociation (HCD)] and MS/MS spectra were acquired with a resolution of 17,500 with AGC target value of 5000, a maximal injection time of 100 ms, and the lowest mass fixed at m/z 120, in centroid mode. Dynamic exclusion duration was 30 s.

SEQUEST search algorithm in Proteome Discoverer software (Thermo Fisher Scientific) was used for peak extraction and protein identification with the mouse reference proteome of UniProtKB database (released 10_2016 with 16954 entries). Allowed error tolerances were 15 ppm and 0.05 Da for the precursor and fragment ions, respectively. Database searches were limited to fully tryptic peptides allowing two missed, and carbamidomethyl +57.021 Da (C) of cysteine residue was set as fixed, and oxidation of methionine +15.995 Da (M) as dynamic modifications. For peptide identification, false discovery rate (FDR) was set to <0.05. The high-confidence protein–protein interactions were identified using stringent filtering against EGFP control samples. The bait (Strep-tag)-normalized relative protein abundances were calculated from the spectral counts.

For phosphoprotein analysis, *Tln1*$^{-/-}$*Tln2*$^{-/-}$ cells were transfected with endotoxin-free plasmid DNA by the Neon transfection system in five parallel reactions of 1×10^6 cells and 5 µg plasmid DNA. To synchronize the state of cell spreading, transfected cells were detached 48 h after transfection and

incubated on a fresh cell culture dish for 150 min. Cells were washed with cold PBS and lysed in 800 µl cooled 50 mM NH_4HCO_3 buffer supplemented with 8 M urea, 1 mM sodium orthovanadate, 1× PhosSTOP phosphatase inhibitor cocktail (Merck, 000000004906845001) and 1:500 protease inhibitor cocktail (Merck, P8430). Lysates were sonicated for 10 min in a cooled water bath sonicator (Diagenode Bioruptor) and cleared by centrifugation (16,000 ***g***, 15 min). For phosphopeptide enrichment, 400 µg of total protein was used. The proteins were reduced with Tris(2-carboxyethyl)phosphine (TCEP; Sigma-Aldrich), alkylated with iodoacetamide, trypsin digested with Sequencing-Grade Modified Trypsin (Promega) using a 1:100 enzyme:protein ratio at 37°C overnight and then desalted with C18 microspin columns (Nest Group). Phosphopeptide enrichment was performed using Ti^{4+}-IMAC. The IMAC material was prepared and used essentially as described (Zhou et al., 2013). Briefly, Ti^{4+}-IMAC beads were loaded onto GELoader tips (Thermo Fisher Scientific) and conditioned with loading buffer [80% ACN, 6% trifluoroacetic acid (TFA)]. The protein digests were dissolved in loading buffer and added into the spin tips. The columns were washed first with 50% ACN, 0.1% TFA with 200 mM NaCl and then without salt. The bound phosphopeptides were eluted with 10% ammonia, followed by purification with C18 microspin columns before LC-MS/MS analysis.

The LC-MS/MS analysis of phosphorylated peptides was performed using the instrumentation described above. The phosphopeptide sample was loaded into a C18-packed precolumn (Acclaim PepMap™100, 100 µm×2 cm, 3 µm, 100 Å; Thermo Fisher Scientific) in buffer A [1% ACN/0.1% formic acid (FA)]. Peptides were transferred onward to a C18-packed analytical column (Acclaim PepMap™100, 75 µm×15 cm, 2 µm, 100 Å) and separated by a 120-min linear gradient from 5% to 35% of buffer B (98% ACN and 0.1% FA in HPLC-grade water) at a flow rate of 300 nl/min. The total measurement time was 140 min per sample. The mass spectrometry analysis was performed as data-dependent acquisition in positive-ion mode. MS spectra were acquired from m/z 300 to m/z 2000 with a resolution of 70,000, with full AGC target value of 3,000,000 ions and a maximal injection time of 120 ms in profile mode. The ten most abundant ions with charge states from 2+ to 7+ were selected for subsequent fragmentation (HCD), and MS/MS spectra were acquired with a resolution of 17,500, with an AGC target value of 5000, a maximal injection time of 120 ms and the lowest mass fixed at m/z 120 in centroid mode. Dynamic exclusion duration was 30 s. Three fully independent replicates were performed for each talin protein and control transfection.

Raw data were processed with MaxQuant version 1.6.0.16 (Cox and Mann, 2008). MS spectra were compared against the mouse component of the UniProtKB database (release 2017_09 with 16,970 entries) using the Andromeda search engine (Cox et al., 2011). Carbamidomethylation (+57.021 Da) of cysteine residues was used as static modification. Phosphorylation of serine/threonine/tyrosine (+79.966 Da) and oxidation (+15.994 Da) of methionine were used as dynamic modification. Precursor mass tolerance and fragment mass tolerance were set to less than 20 ppm and 0.1 Da, respectively. A maximum of two missed cleavages was allowed. The results were filtered to a maximum FDR of 0.05. DAVID 6.8 was used for the functional annotation enrichment analysis and JVenn tool to visualize the overlaps in the phosphorylation data (Huang et al., 2009; Bardou et al., 2014).

Quantification and statistical analysis

The statistical parameters, including the number of analyzed cells and the number of independent experimental repeats, are presented in each figure legend. In all graphs, bar height and error bars denote data mean and s.d., respectively. The statistical significance of all results was analyzed with one-way ANOVA with Bonferroni test. $P<0.05$ was considered statistically significant. In all figures, ns, not significant; $*P<0.05$, $**P<0.01$, $***P<0.001$. Statistical analysis was performed in Prism 5.02 (GraphPad Software).

Acknowledgements

The use of equipment and expert services of the BioMediTech Microscopy core facility at the University of Tampere is gratefully acknowledged. We thank Prof. Reinhard Fässler and Dr Carsten Grashoff (Max Planck Institute of Biochemistry) for help with the *Tln1*$^{-/-}$*Tln2*$^{-/-}$ cells; Dr Armando del Rio (Imperial College London) for help with the vinculin expression constructs; Prof. Michael Sheetz (National University of Singapore) for providing the mouse wild-type talin expression construct; Prof. Bernhard Wehrle-Haller (University of Geneva) and Dr Teemu Ihalainen (University of Tampere) for helpful comments; Ulla Kiiskinen, Niklas Kähkönen, Latifeh Azizi and Merja Jokela (University of Tampere) for skillful technical assistance; and Biocenter Finland for infrastructure support.

Competing interests

The authors declare no competing or financial interests.

Author contributions

Conceptualization: R.R., T.Ö., M.V., V.P.H.; Methodology: R.R., T.Ö., P.T.; Investigation: R.R., T.Ö., P.T., V.P.H.; Data curation: R.R.; Writing - original draft: R.R.; Writing - review & editing: R.R., T.Ö., P.T., M.V., V.P.H.; Visualization: R.R.; Supervision: M.V., V.P.H.; Project administration: V.P.H.; Funding acquisition: M.V., V.P.H.

Funding

This research was supported by the Academy of Finland [290506, 273192 and 136288 to V.P.H.] and Suomen Kulttuurirahasto [50131349 and 50171546 to R.R.].

Supplementary information

Supplementary information available online at
http://jcs.biologists.org/lookup/doi/10.1242/jcs.226514.supplemental

References

Arthur, W. T. and Burridge, K. (2001). RhoA inactivation by p190RhoGAP regulates cell spreading and migration by promoting membrane protrusion and polarity. *Mol. Biol. Cell* **12**, 2711-2720.

Arthur, W. T., Petch, L. A. and Burridge, K. (2000). Integrin engagement suppresses RhoA activity via a c-Src-dependent mechanism. *Curr. Biol.* **10**, 719-722.

Atherton, P., Stutchbury, B., Wang, D.-Y., Jethwa, D., Tsang, R., Meiler-Rodriguez, E., Wang, P., Bate, N., Zent, R., Barsukov, I. L. et al. (2015). Vinculin controls talin engagement with the actomyosin machinery. *Nat. Commun.* **6**, e10038.

Austen, K., Ringer, P., Mehlich, A., Chrostek-Grashoff, A., Kluger, C., Klingner, C., Sabass, B., Zent, R., Rief, M. and Grashoff, C. (2015). Extracellular rigidity sensing by talin isoform-specific mechanical linkages. *Nat. Cell Biol.* **17**, 1597-1606.

Bardou, P., Mariette, J., Escudié, F., Djemiel, C. and Klopp, C. (2014). jvenn: an interactive Venn diagram viewer. *BMC Bioinformatics* **15**, 293.

Bell, S. and Terentjev, E. M. (2017). Focal adhesion kinase: the reversible molecular Mechanosensor. *Biophys. J.* **112**, 2439-2450.

Benito-Jardón, M., Klapproth, S., Gimeno-Lluch, I., Petzold, T., Bharadwaj, M., Müller, D. J., Zuchtriegel, G., Reichel, C. A. and Costell, M. (2017). The fibronectin synergy site re-enforces cell adhesion and mediates a crosstalk between integrin classes. *eLife* **6**, e22264.

Brindle, N. P. J., Holt, M. R., Davies, J. E., Price, C. J. and Critchley, D. R. (1996). The focal-adhesion vasodilator-stimulated phosphoprotein (VASP) binds to the proline-rich domain in vinculin. *Biochem. J.* **318**, 753-757.

Bun, P., Liu, J. J., Turlier, H., Liu, Z. Z., Uriot, K., Joanny, J.-F. and Coppey-Moisan, M. (2014). Mechanical checkpoint for persistent cell polarization in adhesion-naive fibroblasts. *Biophys. J.* **107**, 324-335.

Carisey, A. and Ballestrem, C. (2011). Vinculin, an adapter protein in control of cell adhesion signalling. *Eur. J. Cell Biol.* **90**, 157-163.

Carisey, A., Tsang, R., Greiner, A. M., Nijenhuis, N., Heath, N., Nazgiewicz, A., Kemkemer, R., Derby, B., Spatz, J. and Ballestrem, C. (2013). Vinculin regulates the recruitment and release of core focal adhesion proteins in a force-dependent manner. *Curr. Biol.* **23**, 271-281.

Cohen, D. M., Chen, H., Johnson, R. P., Choudhury, B. and Craig, S. W. (2005). Two distinct head-tail interfaces cooperate to suppress activation of vinculin by talin. *J. Biol. Chem.* **280**, 17109-17117.

Coll, J. L., Ben-Ze'ev, A., Ezzell, R. M., Rodriguez Fernandez, J. L., Baribault, H., Oshima, R. G. and Adamson, E. D. (1995). Targeted disruption of vinculin genes in F9 and embryonic stem cells changes cell morphology, adhesion, and locomotion. *Proc. Natl. Acad. Sci. USA* **92**, 9161-9165.

Coutts, A. S., MacKenzie, E., Griffith, E. and Black, D. M. (2003). TES is a novel focal adhesion protein with a role in cell spreading. *J. Cell Sci.* **116**, 897-906.

Cox, J. and Mann, M. (2008). MaxQuant enables high peptide identification rates, individualized p.p.b.-range mass accuracies and proteome-wide protein quantification. *Nat. Biotechnol.* **26**, 1367-1372.

Cox, J., Neuhauser, N., Michalski, A., Scheltema, R. A., Olsen, J. V. and Mann, M. (2011). Andromeda: a peptide search engine integrated into the MaxQuant environment. *J. Proteome Res.* **10**, 1794-1805.

Del Rio, A., Perez-Jimenez, R., Liu, R., Roca-Cusachs, P., Fernandez, J. M. and Sheetz, M. P. (2009). Stretching single talin rod molecules activates vinculin binding. *Science* **323**, 638-641.

Elosegui-Artola, A., Oria, R., Chen, Y., Kosmalska, A., Pérez-González, C., Castro, N., Zhu, C., Trepat, X. and Roca-Cusachs, P. (2016). Mechanical regulation of a molecular clutch defines force transmission and transduction in response to matrix rigidity. *Nat. Cell Biol.* **18**, 540-548.

Gao, J., Huang, M., Lai, J., Mao, K., Sun, P., Cao, Z., Hu, Y., Zhang, Y., Schulte, M. L., Jin, C. et al. (2017). Kindlin supports platelet integrin αIIbβ3 activation by interacting with paxillin. *J. Cell Sci.* **130**, 3764-3775.

Glogauer, M., Arora, P., Chou, D., Janmey, P. A., Downey, G. P. and Mcculloch, C. A. G. (1998). The role of actin-binding protein 280 in integrin-dependent mechanoprotection. *J. Biol. Chem.* **273**, 1689-1698.

Gough, R. E. and Goult, B. T. (2018). The tale of two talins - two isoforms to fine-tune integrin signalling. *FEBS Lett.* **592**, 2108-2125.

Goult, B. T., Zacharchenko, T., Bate, N., Tsang, R., Hey, F., Gingras, A. R., Elliott, P. R., Roberts, G. C. K., Ballestrem, C., Critchley, D. R. et al. (2013). RIAM and vinculin binding to talin are mutually exclusive and regulate adhesion assembly and turnover. *J. Biol. Chem.* **288**, 8238-8249.

Guo, B. and Guilford, W. H. (2006). Mechanics of actomyosin bonds in different nucleotide states are tuned to muscle contraction. *Proc. Natl. Acad. Sci. USA* **103**, 9844-9849.

Haining, A. W. M., von Essen, M., Attwood, S. J., Hytönen, V. P. and del Río Hernández, A. (2016). All subdomains of the Talin rod are mechanically vulnerable and may contribute to cellular mechanosensing. *ACS Nano* **10**, 6648-6658.

Haining, A. W. M., Rahikainen, R., Cortes, E., Lachowski, D., Rice, A., von Essen, M., Hytönen, V. P. and del Río Hernández, A. (2018). Mechanotransduction in talin through the interaction of the R8 domain with DLC1. *PLoS Biol.* **16**, e2005599.

Hayakawa, K., Tatsumi, H. and Sokabe, M. (2011). Actin filaments function as a tension sensor by tension-dependent binding of cofilin to the filament. *J. Cell Biol.* **195**, 721-727.

Horton, E. R., Byron, A., Askari, J. A., Ng, D. H. J., Millon-Frémillon, A., Robertson, J., Koper, E. J., Paul, N. R., Warwood, S., Knight, D. et al. (2015). Definition of a consensus integrin adhesome and its dynamics during adhesion complex assembly and disassembly. *Nat. Cell Biol.* **17**, 1577-1587.

Huang, D. W., Sherman, B. T. and Lempicki, R. A. (2009). Systematic and integrative analysis of large gene lists using DAVID bioinformatics resources. *Nat. Protoc.* **4**, 44-57.

Huang, D. L., Bax, N. A., Buckley, C. D., Weis, W. I. and Dunn, A. R. (2017). Vinculin forms a directionally asymmetric catch bond with F-actin. *Science* **357**, 703-706.

Hüttelmaier, S., Mayboroda, O., Harbeck, B., Jarchau, T., Jockusch, B. M. and Rüdiger, M. (1998). The interaction of the cell-contact proteins VASP and vinculin is regulated by phosphatidylinositol-4,5-bisphosphate. *Curr. Biol.* **8**, 479-488.

Hytönen, V. P. and Vogel, V. (2008). How force might activate Talin's Vinculin binding sites: SMD reveals a structural mechanism. *PLoS Comput. Biol.* **4**, e24.

Hytönen, V. P. and Wehrle-Haller, B. (2014). Protein conformation as a regulator of cell-matrix adhesion. *Phys. Chem. Chem. Phys.* **16**, 6342-6357.

Hytönen, V. P. and Wehrle-Haller, B. (2016). Mechanosensing in cell–matrix adhesions – converting tension into chemical signals. *Exp. Cell Res.* **343**, 35-41.

Kong, F., García, A. J., Mould, A. P., Humphries, M. J. and Zhu, C. (2009). Demonstration of catch bonds between an integrin and its ligand. *J. Cell Biol.* **185**, 1275-1284.

Lafuente, E. M., van Puijenbroek, A. A. F. L., Krause, M., Carman, C. V., Freeman, G. J., Berezovskaya, A., Constantine, E., Springer, T. A., Gertler, F. B. and Boussiotis, V. A. (2004). RIAM, an Ena/VASP and profilin ligand, interacts with Rap1-GTP and mediates Rap1-induced adhesion. *Dev. Cell* **7**, 585-595.

Lawson, C., Lim, S.-T., Uryu, S., Chen, X. L., Calderwood, D. A. and Schlaepfer, D. D. (2012). FAK promotes recruitment of talin to nascent adhesions to control cell motility. *J. Cell Biol.* **196**, 223-232.

Liu, J., Wang, Y., Goh, W. I., Goh, H., Baird, M. A., Ruehland, S., Teo, S., Bate, N., Critchley, D. R., Davidson, M. W. et al. (2015). Talin determines the nanoscale architecture of focal adhesions. *Proc. Natl Acad. Sci. USA* **112**, E4864-E4873.

Liu, X., Salokas, K., Tamene, F., Jiu, Y., Weldatsadik, R. G., Öhman, T. and Varjosalo, M. (2018). An AP-MS- and BioID-compatible MAC-tag enables comprehensive mapping of protein interactions and subcellular localizations. *Nat. Commun.* **9**, 1188.

Margadant, F., Chew, L. L., Hu, X., Yu, H., Bate, N., Zhang, X. and Sheetz, M. (2011). Mechanotransduction in vivo by repeated talin stretch-relaxation events depends upon vinculin. *PLoS Biol.* **9**, e1001223.

Meacci, G., Wolfenson, H., Liu, S., Stachowiak, M. R., Iskratsch, T., Mathur, A., Ghassemi, S., Gauthier, N., Tabdanov, E., Lohner, J. et al. (2016). α-Actinin links extracellular matrix rigidity-sensing contractile units with periodic cell-edge retractions. *Mol. Biol. Cell* **27**, 3471-3479.

Meijering, E., Dzyubachyk, O. and Smal, I. (2012). Methods for cell and particle tracking. *Methods Enzymol.* **504**, 183-200.

Prager-Khoutorsky, M., Lichtenstein, A., Krishnan, R., Rajendran, K., Mayo, A., Kam, Z., Geiger, B. and Bershadsky, A. D. (2011). Fibroblast polarization is a matrix-rigidity-dependent process controlled by focal adhesion mechanosensing. *Nat. Cell Biol.* **13**, 1457-1465.

Rahikainen, R., von Essen, M., Schaefer, M., Qi, L., Azizi, L., Kelly, C., Ihalainen, T. O., Wehrle-Haller, B., Bastmeyer, M., Huang, C. et al. (2017). Mechanical stability of talin rod controls cell migration and substrate sensing. *Sci. Rep.* **7**, 3571.

Rapsomaniki, M. A., Kotsantis, P., Symeonidou, I.-E., Giakoumakis, N.-N., Taraviras, S. and Lygerou, Z. (2012). easyFRAP: an interactive, easy-to-use tool for qualitative and quantitative analysis of FRAP data. *Bioinformatics* **28**, 1800-1801.

Roux, K. J., Kim, D. I., Burke, B. and May, D. G. (2018). BioID: a screen for protein-protein interactions. *Curr. Protoc. Protein Sci.* **569**, 19.23.1-19.23.15.

Sala, S., Van Troys, M., Medves, S., Catillon, M., Timmerman, E., Staes, A., Schaffner-Reckinger, E., Gevaert, K. and Ampe, C. (2017). Expanding the Interactome of TES by Exploiting TES Modules with Different Subcellular Localizations. *J. Proteome Res.* **16**, 2054-2071.

Schneider, C. A., Rasband, W. S. and Eliceiri, K. W. (2012). NIH Image to ImageJ: 25 years of image analysis. *Nat. Methods* **9**, 671-675.

Seong, J., Tajik, A., Sun, J., Guan, J.-L., Humphries, M. J., Craig, S. E., Shekaran, A., Garcia, A. J., Lu, S., Lin, M. Z. et al. (2013). Distinct biophysical mechanisms of focal adhesion kinase mechanoactivation by different extracellular matrix proteins. *Proc. Natl. Acad. Sci. USA* **110**, 19372-19377.

Stutchbury, B., Atherton, P., Tsang, R., Wang, D.-Y. and Ballestrem, C. (2017). Distinct focal adhesion protein modules control different aspects of mechanotransduction. *J. Cell Sci.* **130**, 1612-1624.

Subauste, M. C., Pertz, O., Adamson, E. D., Turner, C. E., Junger, S. and Hahn, K. M. (2004). Vinculin modulation of paxillin-FAK interactions regulates ERK to control survival and motility. *J. Cell Biol.* **165**, 371-381.

Sun, Z., Tseng, H.-Y., Tan, S., Senger, F., Kurzawa, L., Dedden, D., Mizuno, N., Wasik, A. A., Thery, M., Dunn, A. R. et al. (2016). Kank2 activates talin, reduces force transduction across integrins and induces central adhesion formation. *Nat. Cell Biol.* **18**, 941-953.

Theodosiou, M., Widmaier, M., Böttcher, R. T., Rognoni, E., Veelders, M., Bharadwaj, M., Lambacher, A., Austen, K., Müller, D. J., Zent, R. et al. (2016). Kindlin-2 cooperates with talin to activate integrins and induces cell spreading by directly binding paxillin. *eLife* **5**, e10130.

Thievessen, I., Thompson, P. M., Berlemont, S., Plevock, K. M., Plotnikov, S. V., Zemljic-Harpf, A., Ross, R. S., Davidson, M. W., Danuser, G., Campbell, S. L. et al. (2013). Vinculin-actin interaction couples actin retrograde flow to focal adhesions, but is dispensable for focal adhesion growth. *J. Cell Biol.* **202**, 163-177.

Thievessen, I., Fakhri, N., Steinwachs, J., Kraus, V., Mcisaac, R. S., Gao, L., Chen, B.-C., Baird, M. A., Davidson, M. W., Betzig, E. et al. (2015). Vinculin is required for cell polarization, migration, and extracellular matrix remodeling in 3D collagen. *FASEB J.* **29**, 4555-4567.

Tsubouchi, A., Sakakura, J., Yagi, R., Mazaki, Y., Schaefer, E., Yano, H. and Sabe, H. (2002). Localized suppression of RhoA activity by Tyr31/118-phosphorylated paxillin in cell adhesion and migration. *J. Cell Biol.* **159**, 673-683.

Wehrle-Haller, B. (2012). Structure and function of focal adhesions. *Curr. Opin. Cell Biol.* **24**, 116-124.

Weinberg, S. H., Mair, D. B. and Lemmon, C. A. (2017). Mechanotransduction dynamics at the cell-matrix interface. *Biophys. J.* **112**, 1962-1974.

Wolfenson, H., Meacci, G., Liu, S., Stachowiak, M. R., Iskratsch, T., Ghassemi, S., Roca-Cusachs, P., O'Shaughnessy, B., Hone, J. and Sheetz, M. P. (2016). Tropomyosin controls sarcomere-like contractions for rigidity sensing and suppressing growth on soft matrices. *Nat. Cell Biol.* **18**, 33-42.

Xu, W. and Baribault, H. (1998). Vinculin knockout results in heart and brain defects during embryonic development. *Development* **125**, 327-337.

Yamashiro, S., Tanaka, S., Mcmillen, L. M., Taniguchi, D., Vavylonis, D. and Weaver, V. M. (2018). Myosin-dependent actin stabilization as revealed by single-molecule imaging of actin turnover. *Mol. Biol. Cell* **29**, 1941-1947.

Ye, N., Verma, D., Meng, F., Davidson, M. W., Suffoletto, K. and Hua, S. Z. (2014). Direct observation of α-actinin tension and recruitment at focal adhesions during contact growth. *Exp. Cell Res.* **327**, 57-67.

Zacharchenko, T., Goult, B. T., Jethwa, D., Almeida, T. B., Ballestrem, C., Critchley, D. R., Lowy, D. R. and Barsukov, I. L. (2016). LD motif recognition by Talin: structure of the Talin-DLC1 complex. *Structure* **24**, 1130-1141.

Zaidel-Bar, R. and Geiger, B. (2010). The switchable integrin adhesome. *J. Cell Sci.* **123**, 1385-1388.

Zhang, X., Jiang, G., Cai, Y., Monkley, S. J., Critchley, D. R. and Sheetz, M. P. (2008). Talin depletion reveals independence of initial cell spreading from integrin activation and traction. *Nat. Cell Biol.* **10**, 1062-1068.

Zhou, H., Ye, M., Dong, J., Corradini, E., Cristobal, A., Heck, A. J. R., Zou, H. and Mohammed, S. (2013). Robust phosphoproteome enrichment using monodisperse microsphere–based immobilized titanium (IV) ion affinity chromatography. *Nat. Protoc.* **8**, 461-480.

Zhou, J., Aponte-Santamaría, C., Sturm, S., Bullerjahn, J. T., Bronowska, A., Gräter, F. and Kasson, P. M. (2015). Mechanism of focal adhesion kinase mechanosensing. *PLoS Comput. Biol.* **11**, e1004593.

Supplemental information

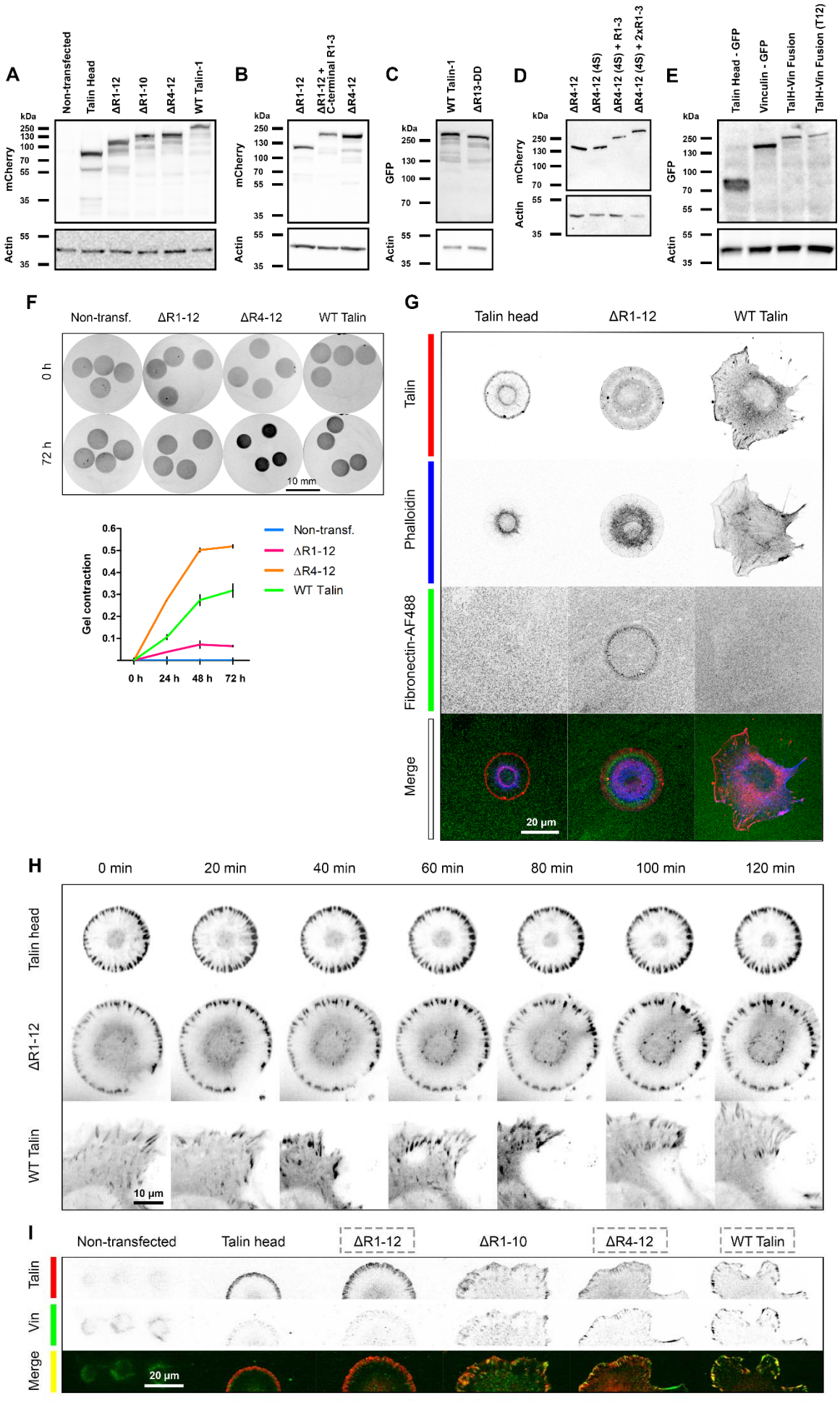

Figure S1, Related to Figure 1. (A - E) Western blot analysis for different talin forms. To confirm the correct expression of modified talin proteins at comparable expression levels, lysates of transiently transfected *Tln1-/-Tln2-/-* cells were analyzed by Western blotting with anti-mCherry, anti-GFP and anti-actin. (F) The macroscopic contraction of collagen-I matrices embedded with cells expressing different talin forms was followed over 72 hours. Note how both wild type talin and the ΔR4-12 protein were able to macroscopically contract the collagen-I matrix, while the ΔR1-12 protein did not allow comparable gel contraction. (G) Fibronectin reorganization assay. *Tln1-/-Tln2-/-* cells expressing the talin head domain, ΔR1-12 or wild type talin were plated on glass coverslips coated with AlexaFluor488 labeled fibronectin and fixed after 120 minutes. In the inversed coloring of the AlexaFluor488-fibronecting image, increased accumulation of fibronectin is indicated by a darker color. Note how the ΔR1-12 protein is able to mediate the relocation of fluorescent fibronectin from the distal end of the adhesion sites to the central end of these adhesions. (H) Time-lapse image series for cells shown in Figure 1I. *Tln1-/-Tln2-/-* cells expressing Talin-GFP fusion proteins were imaged for 120 min using spinning disk confocal microscope. (I) Representative images of vinculin immunostaining. Close-ups of the samples marked with dashed boxes and quantification of vinculin intensity are presented in Figure 1J - M.

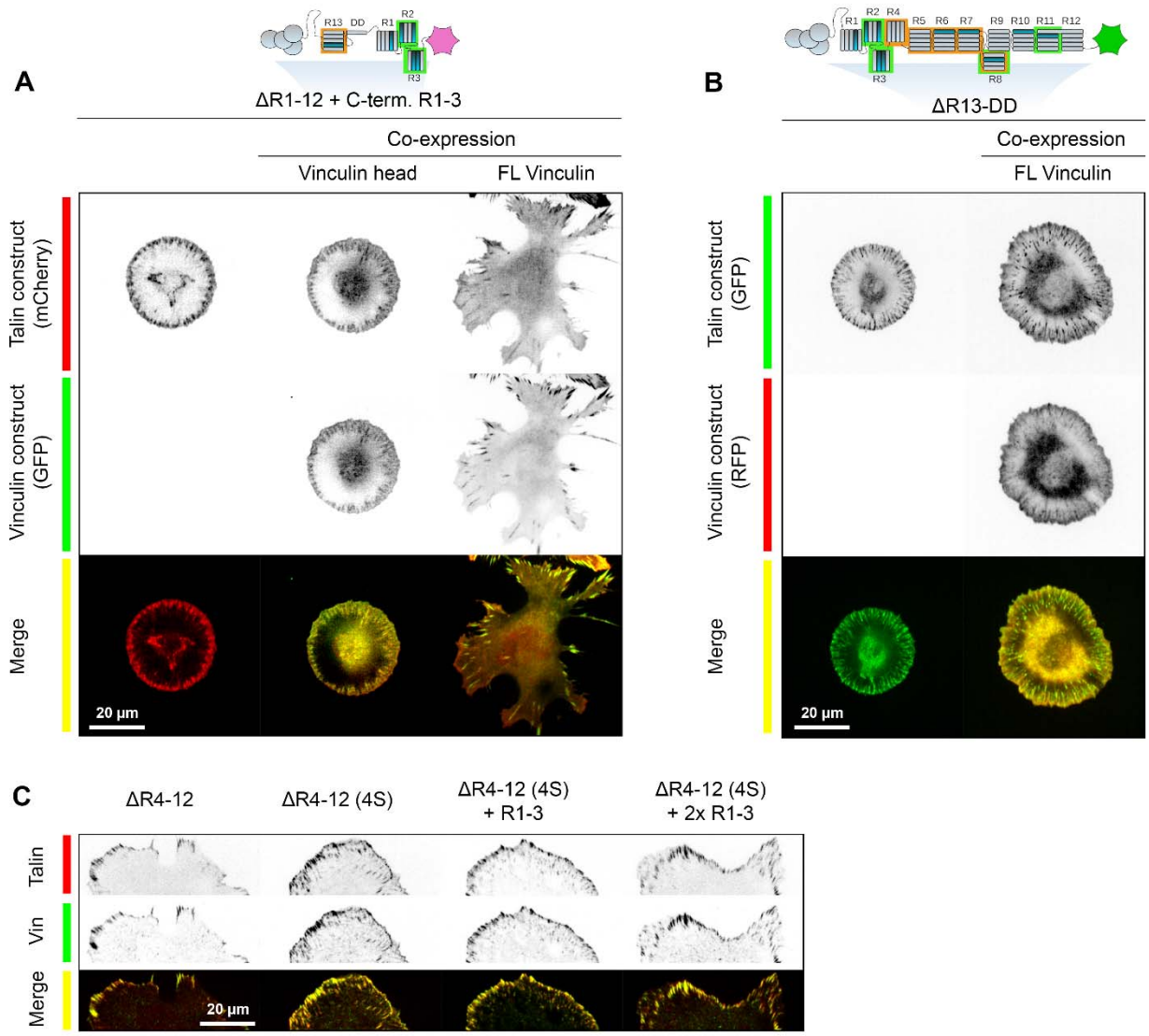

Figure S2, Related to Figure 2. (A) Co-expression of full-length vinculin, but not its head domain, facilitates the polarization of cells expressing the ΔR1-12 + C-term. R1-3 talin form. *Tln1-/-Tln2-/-* cells were co-transfected with the ΔR1-12 + C-term. R1-3 and either full-length vinculin or vinculin head domain (residues 1 - 255) tagged with GFP. The co-expressed vinculin head domain co-localized with the talin protein, but was unable to facilitate cell polarization. Co-expression of either full-length vinculin or its auto-inhibition deficient mutant T12 (not shown) resulted in cell polarization. (B) Co-expression of vinculin tagged with RFP with talin ΔR13-DD protein tagged with GFP. (C) Representative images of vinculin immunostaining of cells expressing destabilized talin proteins.

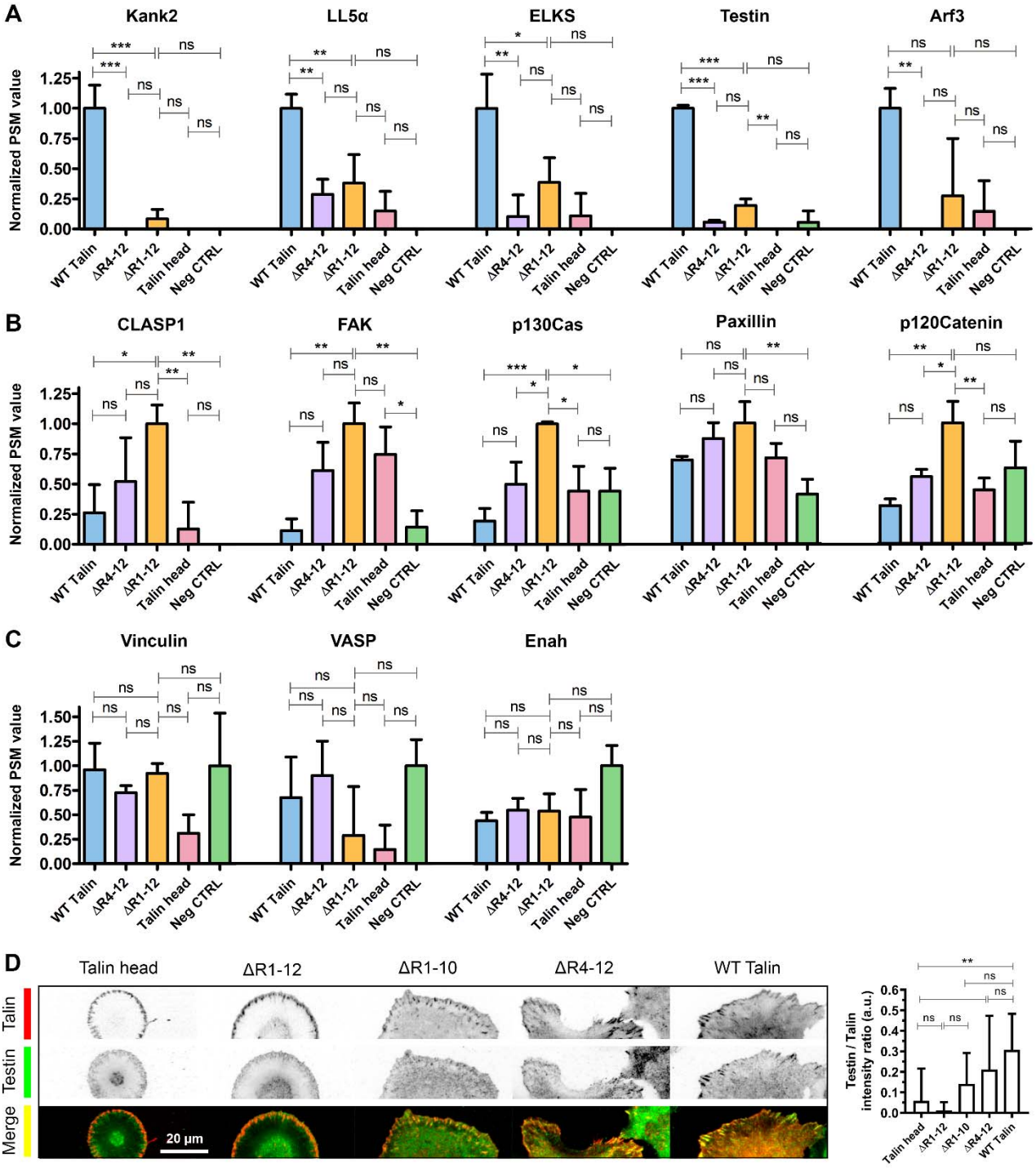

Figure S3, Related to Figure 3. BioID analysis for cells expressing modified talin proteins. (A) Normalized peptide spectrum match (PSM) values for proteins with the highest signal in cells expressing wild type talin. (B) Normalized PSM values for proteins showing the increased signals in cells expressing interactions with the ΔR1-12 protein as compared to the other talin forms. (C) Normalized PSM values for adhesion proteins Vinculin, VASP and Enah. In each graph, PSM values were normalized to the highest value. Bars represent mean PSM values of three replicate MS/MS runs ± standard deviation. (D) Testin immunostaining for *Tln1-/-Tln2-/-* cells expressing different talin proteins. n = 8-13 cells for each talin protein. * = p<0.05, ** = p<0.01, *** = p<0.001

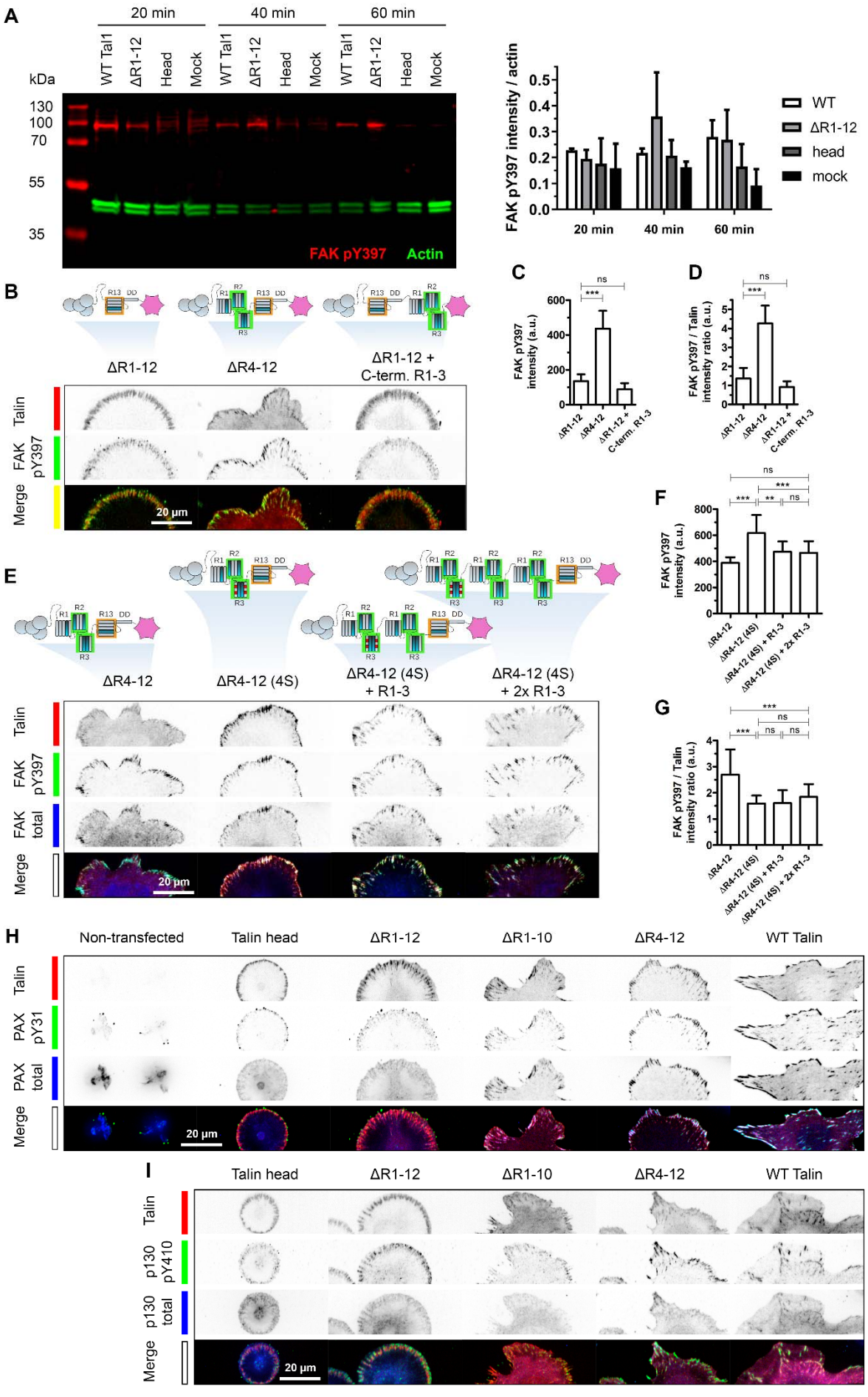

Figure S4, Related to Figure 4. (A) Western blot analysis for FAK activation at different time points after plating cells. Bars represent mean ± standard deviation from two independent experiments. (B - D) Representative images and quantification of FAK pY397 immunostaining for *Tln1-/-Tln2-/-* cells expressing ΔR4-12 or ΔR1-12 + C-term. R1-3 proteins. n = 4 - 22 cells for each talin protein. In C, FAK pY397 intensity in adhesion sites was normalized by the average talin intensity in adhesion sites in each cell. (E – G) Representative images and quantification of FAK pY397 immunostaining for *Tln1-/-Tln2-/-* cells expressing destabilized talin proteins. n = 8 - 16 cells for each talin protein. (H) Representative images of paxillin and paxillin pY31 immunostaining in cells expressing talin different talin proteins. (I) Representative images of p130Cas and p130Cas pY410 immunostaining in cells expressing different talin proteins. In all graphs, bars represent mean ± standard deviation. The statistical significance of all results was analyzed by one-way ANOVA and Bonferroni test, ns = not significant, * = $p<0.05$, ** = $p<0.01$, *** = $p<0.001$.

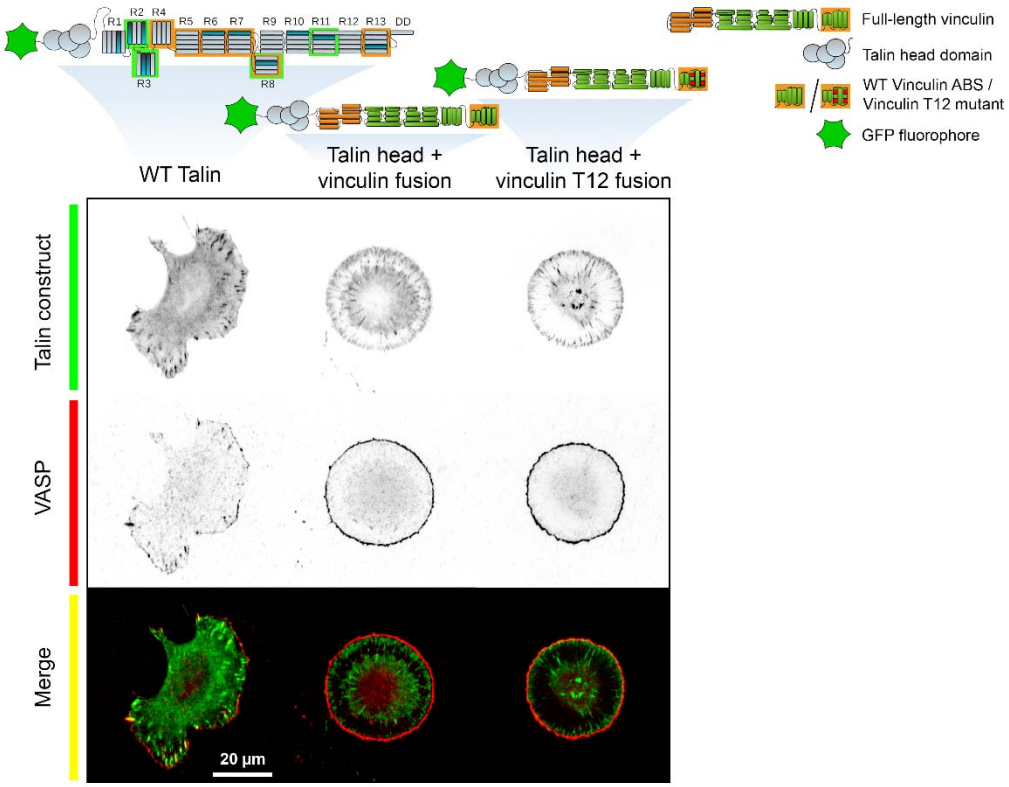

Figure S5, Related to Figure 5. Representative confocal microscope images of *Tln1-/-Tln2-/-* cells expressing wild-type talin or the talin head domain + vinculin fusion proteins. Vinculin (T12) mutant is autoinhibition deficient and has a constitutively active F-actin binding domain. The talin-vinculin fusion protein localized into radial adhesion sites and induced isotropic cell spreading, but did not recruit any VASP into adhesion sites. Instead, VASP strongly localized to the edge of the cell lamellipodium.

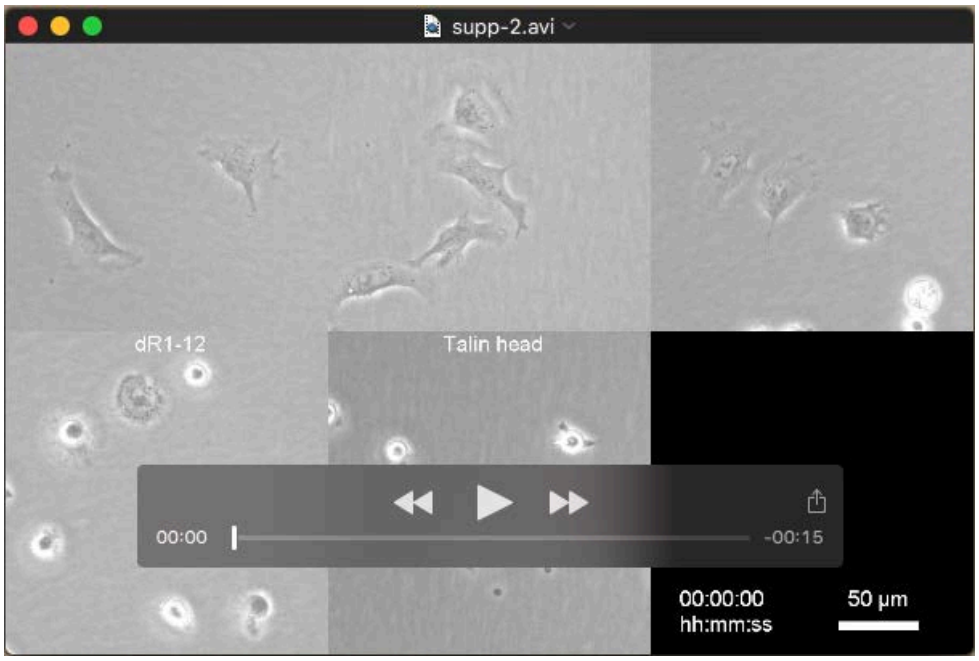

Movie 1, Related to Figure 1E. Time-lapse video of *Tln1-/-Tln2-/-* cells expressing the truncated talin proteins. Cells expressing different talin proteins were plated on a fibronectin-coated polystyrene plate and allowed to attach to the surface for 120 minutes before imaging. Time-lapse series was collected at a 360 seconds interval for 12 hours.

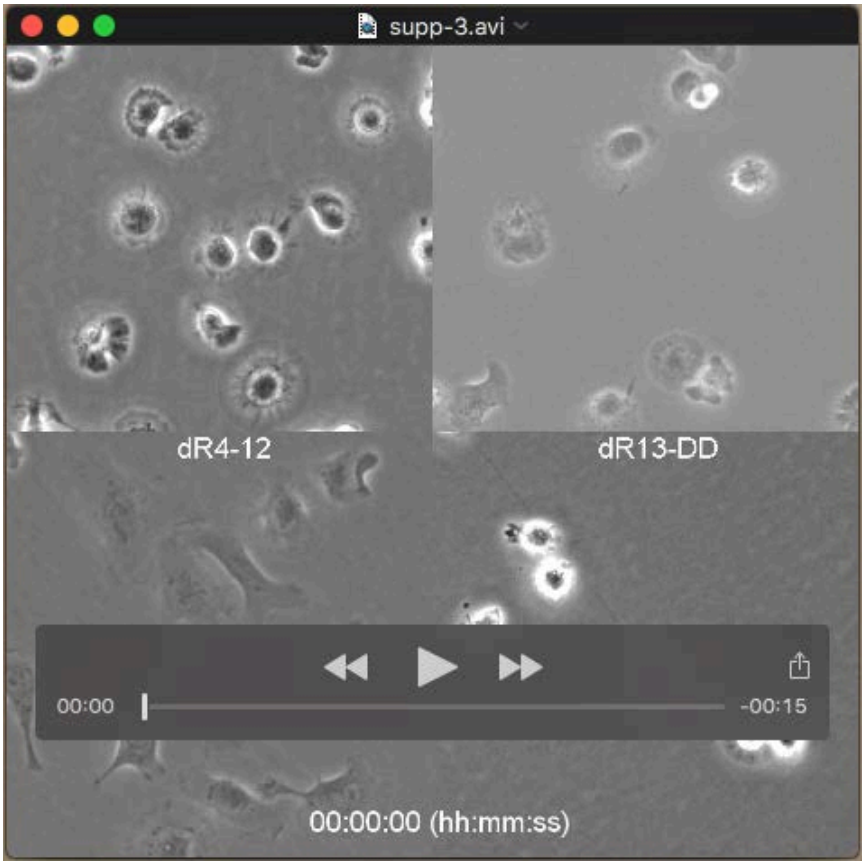

Movie 2, Related to Figure 2A, E. Time-lapse video for *Tln1-/-Tln2-/-* cells expressing the reorganized talin proteins or the ΔR13-DD protein. Cells expressing different talin proteins were plated on a fibronectin-coated polystyrene plate and allowed to attach to the surface for 120 minutes before imaging. Time-lapse series was collected at a 120 seconds interval for 12 hours. The size of each field is 200 μm x 200 μm. Note how the cells expressing the ΔR1-12 + C-terminal R1-3 protein have a non-polarized phenotype identical to cells expressing the ΔR1-12 form.

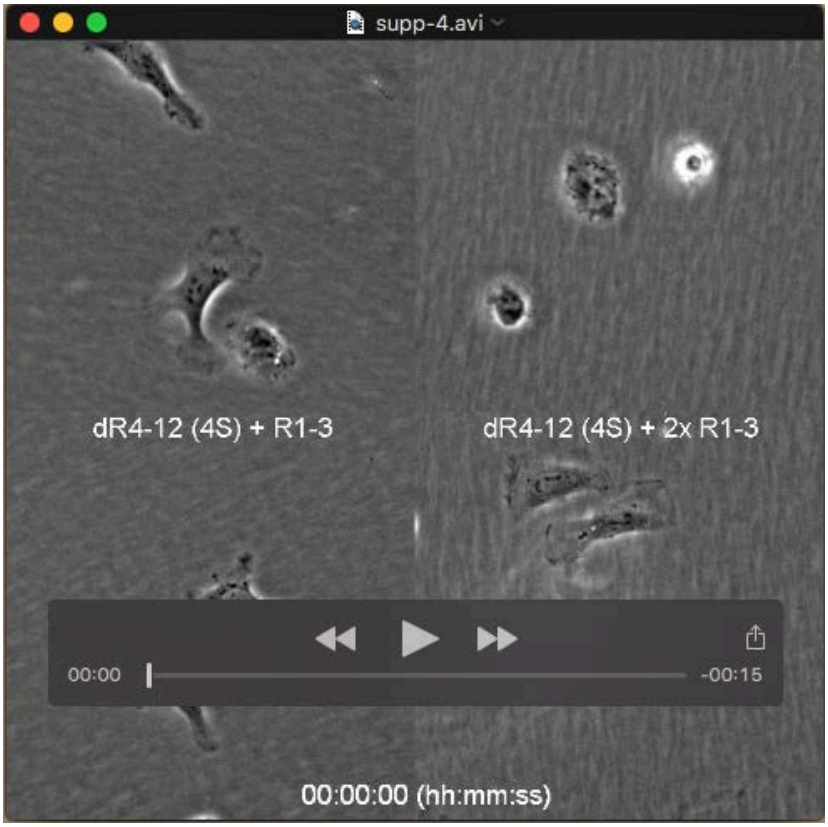

Movie 3, Related to Figure 2I. Time-lapse video for *Tln1-/-Tln2-/-* cells expressing the destabilized and tandem talin proteins presented. Cells expressing different talin proteins were plated on a fibronectin-coated polystyrene plate and allowed to attach to the surface for 120 minutes before imaging. Time-lapse series was collected at a 360 seconds interval for 12 hours. The size of each field is 200 μm x 200 μm. Note how the destabilization of the talin R3 subdomain by point mutations (ΔR4-12 (4S) talin mutant) inhibits cell spreading, polarization and migration. However, this effect is rescued by the addition of non-destabilized talin rod subdomains R1-3 into a tandem configuration (ΔR4-12 (4S) + R1-3 and ΔR4-12 (4S) + 2xR1-3 tandem proteins).

Table S1. Related to Figure S3. Complete list of all proteins identified in the proximity biotinylation analysis. Normalized peptide spectrum match (PSM) values for proteins reliably identified in at least one of the samples. Each sample was analyzed in three replicate MS/MS runs. All PSM values were normalized to the PSM value for the SH-Tag in each run.

Click here to Download Table S1

Table S2, Related to Figure 3. Complete list of all phosphorylated sites reliably identified in at least one of the four studied samples (WT talin, Δ1-12, Talin head, Negative control). Phosphorylated sites identified in at least two out of the three experimental replicates were considered reliable. For each of these sites, the mean intensity of the three experimental replicates was calculated. Detected sites with undetermined intensity values were given an intensity value of zero. #DIV/0 denotes that the given site was not detected in this sample.

Click here to Download Table S2

Table S3, Related to Figure 3. List of phosphorylated sites detected in each sample. Only sites reliably identified in at least one of the four samples are included in the list (see Table S2). Also sites that were detected but whose intensity could not be determined are included.

Click here to Download Table S3

Table S4, Related to Figure 3. Detected phosphorylated sites unique for each sample and common for all samples. Comparison based on sites presented in the Table S3.

Click here to Download Table S4

Table S5, Related to Figure 3. Enrichment analysis for the functional clustering terms of differentially phosphorylated proteins. Enrichment analysis for the functional clustering terms (Gene ontology term Biological Processes) of proteins with one or more differentially phosphorylated sites. See Table S4 for the complete lists of phosphorylated sites.

Click here to Download Table S5

Table S6, Related to Figure 3. Lists of differently phosphorylated proteins identified in the pairwise analysis of phosphorylation sites. List of proteins differently phosphorylated at one or more residues. The mean intensities of each site were compared in two pairs, WT talin vs. ΔR1-12 and ΔR1-12 vs. talin head. A 5-fold increase in the determined intensity was considered to be significant. Sites undetected in one sample and with undetectable signal intensity in the other sample were filtered out. Finally, duplicate hits within each list were filtered out.

Click here to Download Table S6

Table S7, Related to Figure 3. List of the differentially phosphorylated residues in the adhesion proteins presented in Figure 3B. For palladin the exact phosphorylation site could not be determined.

Click here to Download Table S7